Ontario

Ministry of
Transportation

Structural Office

Report SO 93-08

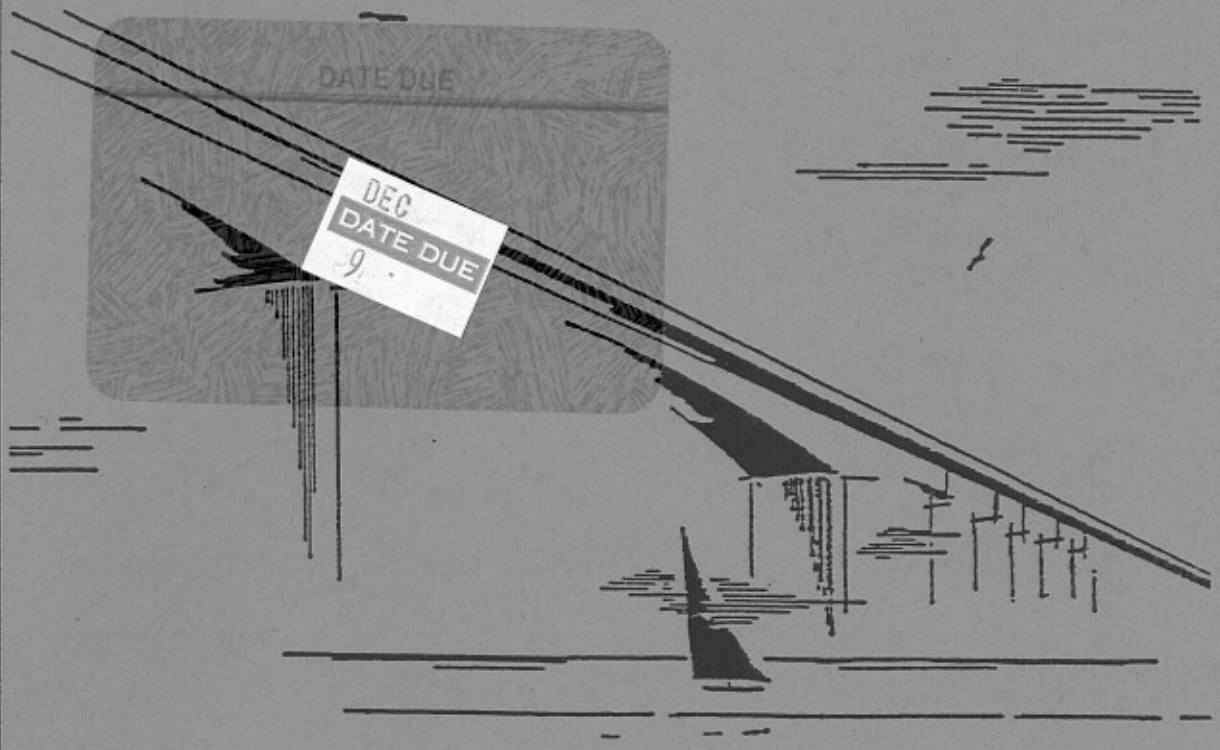

NEW IMPULSE RADAR STRATAGIES

FOR

BRIDGE DECK ASSESSMENT

NEW

IMPULSE RADAR STRATEGIES

FOR BRIDGE DECK ASSESSMENT

by

R. Reel*, T. Tharmabala*, D. Wood*

T. Chung** and C. R. Carter**

*Bridge Management Section,
Structural Office,
Ministry of Transportation, Ontario

**Communications Research Laboratory,
McMaster University,
Hamilton, Ontario

March 1993

*Presented at the 1993 Spring Convention, American Concrete Institute,
Vancouver, B.C. March 28 - April 2, 1993.*

ABSTRACT

Traditional methods of collecting data on the condition of bridges are expensive and time consuming, and the results are not always dependable. Since the early 1980's, the Ministry of Transportation, Ontario (MTO) and the Communications Research Laboratory (CRL) at McMaster University have been involved in the use of impulse radar for the assessment of asphalt-covered bridge decks through a program called Deck Assessment by Radar Technology (DART).

In this paper, a correlation study involving comparisons between the predictions of the DART survey and the actually observed conditions of the decks (after removal of asphalt during rehabilitation) is discussed with emphasis on the processing of the radar waveforms. Since a large volume of radar data is collected from bridge decks, it is important to develop strategies to extract the salient features from the reflected signal. These strategies include: first, a thresholding method and strata plot which are very effective in locating subsurface layers; and, second a differencing technique which has the capability of discriminating between sound concrete and damaged concrete. The comparisons demonstrate that there is a good correlation between the DART survey and the actual condition of bridge decks.

INTRODUCTION

Rehabilitation of asphalt-covered bridge decks requires an accurate estimate of: 1) the asphalt thicknesses across the bridge, 2) the location and extent of concrete deck scaling and delaminations, 3) the depth of concrete cover over the top layer of reinforcement, 4) the half-cell survey data, and 5) the concrete quality, strength, air content and chloride penetration as measured from concrete cores. Currently, the above data are gathered using visual inspection, and a limited amount of physical testing by taking cores, sawn samples and corrosion potential tests. Unfortunately, this approach generally gives insufficient data on the deck condition and leads to cost overruns in bridge deck rehabilitation contracts. A typical cost overrun estimate, incurred by the Ministry of Transportation of Ontario in the year 1986 and presented in Table I[1], exemplifies the difficulty. Hence, there is an urgent need to find alternative methods which could give an improved estimate of the condition of the concrete under the asphalt covered decks.

Since the early 1980's, the Ministry of Transportation of Ontario and the Communication Research Laboratory at McMaster University have been involved in a research program to develop impulse radar as a practical means of assessing the condition of asphalt covered bridge decks through a program called Deck Assessment by Radar Technology (DART)[2-4]. The Ministry has outfitted a van, shown in Fig. 1a, with: a Model PS-24 impulse radar manufactured by Penetradar Corporation of Niagara Falls, New York; a ruggedized 386-based computer with interfacing cards; related test equipment; an engine-driven generator; and a fifth wheel for measuring distance. The impulse radar is monostatic and downward probing, and has a constant flare-angle, variable width open horn antenna, shown in Fig. 1b. The transmitted waveform, illustrated in Fig. 2, has a pulsewidth of approximately one nanosecond (1 ns) in duration and a very high repetition rate.

Impulse signals emitted by the radar propagate through the bridge deck materials and reflect wherever there is a change in the dielectric properties of the propagation medium. These reflected signals contain information on the depth of the asphalt layer, thickness of concrete cover over reinforcement, debonding between asphalt and concrete, and scaling and delamination of the concrete. However, there are many problems associated with the identification procedure. The asphalt thickness and composition can vary since the bridge deck may have two or three layers of asphalt of different makes placed at different times. The location, size, spacing and number of layers of reinforcements can vary along the bridge depending on the structural articulation used in the bridge design.

In the DART program, the application of impulse radar to the evaluation of bridge decks was, until 1991, based on use of the "characteristic W" and "ratio of peaks"[5]. This method worked fairly well if the cover to reinforcement was greater than 50 mm and the asphalt thickness was greater than 50 mm. However, where the cover to reinforcement was less than 50 mm, the technique could not distinguish between delaminations and low covers. This led to a further investigation to enhance the radar technique for better assessment.

In this paper, a correlation study involving comparisons with the DART survey and actual condition of the decks (after removal of asphalt during rehabilitation) is discussed. In particular, a major consideration is devoted to processing techniques used to study the radar waveforms. Large volumes of radar data are collected from bridge decks and it is important to develop strategies to extract the salient features from the reflected signals. Methods discussed here include: a thresholding procedure and strata plot which are very effective in locating subsurface layers; and, a differencing technique which has the capability of differentiating sound and damaged concrete.

PHYSICAL STRUCTURE OF BRIDGE DECKS

There are many different types of bridges in Ontario. The deck reinforcing details can vary considerably depending on the bridge type and the structural idealization assumed by the bridge designer. Some examples of the deck reinforcing details are given in Fig. 3. It is almost impossible to generalize or categorize reinforcing details in a bridge; however, some common details are given here.

1) Old truss type bridges have thin decks supported over closely spaced stringers. These can have light top reinforcement in both directions over the stringers or no top reinforcement between the stringers.

2) Rigid frame (thick slab type) bridges have heavy longitudinal top reinforcement at the abutment/pier areas and light top longitudinal reinforcement at mid spans. Transverse reinforcements for these bridges are usually light and at wide spacing.

3) T-beam rigid frame bridges have similar longitudinal reinforcement to solid rigid frame bridges except that all longitudinal reinforcements may be concentrated within the beam physical width. The thin slab between the beams has similar reinforcement to slab on girder type bridges.

4) Slab on girder type bridges have heavy longitudinal reinforcements at pier locations and light longitudinal reinforcements elsewhere. For these bridges the transverse reinforcements are usually light and widely spaced.

5) Post-tensioned voided deck/post-tensioned box girders bridges have details similar to slab-on-girder bridges except that there could be heavy transverse reinforcements at pier locations. Round voided post-tensioned bridge decks normally have only one layer of longitudinal and transverse reinforcement above the voids. Some may also have nominal transverse post-tensioning.

In all these bridges, the reinforcing bar sizes can vary from 10 mm to 35 mm in diameter. In addition, the reinforcing spacing can vary from 100 mm to 600 mm. The specified cover-to-steel on older bridges varies from 25 mm to 50 mm. Bridges built after the 1970's have a specified cover of 70 $\pm$20 mm. The actual cover differs from the specified cover depending on the construction tolerances and level of supervision and can vary from 5 mm to 150 mm. The reinforcements may be in good condition or have undergone light to very severe corrosion. Older bridges do not have any waterproofing whereas newer bridges do have waterproofing systems, the types include: bitumastic, fabric, and hot applied rubberized asphalt membrane.

From the perspective of impulse radar, a bridge deck may be viewed as a layered structure (asphalt, membrane, concrete, rebars and so on) in which there will be reflections from every layer of material including the different layers of asphalt and reinforcement. In order to represent the reflected

signal, **r(t)**, it is necessary to consider each layer in turn starting with the surface reflection from the top of the asphalt layer and continuing down to the reflection from the reinforcement. Figure 4(a) illustrates a typical asphalt-covered bridge deck structure with the related reflected impulse radar waveform depicted in Fig. 4(b). The equation describing these reflections is

$$r(t)=\rho_A s(t)+\rho_C(1-\rho_A^2)s(t-2T_A)+\rho_R(1-\rho_C^2)(1-\rho_A^2)s(t-2T_A-2T_C) \quad (1)$$

where: **s(t)** is the transmitted signal, as depicted in Fig. 2, ρ_A is the reflection coefficient between air and the asphalt; ρ_C is the reflection coefficient between the asphalt and the concrete; ρ_R is the effective reflection coefficient of the rebars; T_A is the time delay for the signal to propagate from the asphalt surface down to the concrete surface; and T_C is the time delay for the signal to propagate from the concrete surface down to the rebar layer.

Now, in general, the relative dielectric constant ϵ_r and the reflection coefficient ρ are related by

$$\epsilon_r=[\frac{(1-p)}{(1+p)}]^2 \quad (2)$$

Also, the time delay T in any material of thickness D and relative dielectric constant ϵ_r is given by

$$T=\frac{2D\sqrt{\epsilon_r}}{c} \quad (3)$$

where c is the velocity of light. The relative dielectric constants of asphalt and concrete can be evaluated by means already described[4]. Consequently, by measuring the time delays and amplitudes of the peaks from the reflected signal described by Fig. 4(b), the thickness of asphalt and concrete cover over reinforcement can be deduced from (3).

In normal operation, the vehicle is driven along the length of the bridge deck at approximately 5 km/h and data waveforms are collected at 100 mm intervals along the path. Figure 5 provides an actual waterfall plot of reflected waveforms taken at 100 mm intervals along one line of a bridge deck as measured by the fifth wheel. In this plot, the reflections from the air-asphalt boundary are aligned which then leads to identification of the asphalt-concrete interface, as shown. The top rebar layer can also be seen, although its identification is more difficult than that of the concrete surface. The bottom of the deck is clearly defined by the negative-going peaks near the ends of the traces. Other reflections can be useful, such as the reflection from the lower layer of reinforcement.

PROCESSING STRATEGIES

Waterfall Plots

Figure 5 demonstrates the strength in presenting large amounts of data by using the waterfall plot technique. An important feature of this method is that it is possible to identify the asphalt-concrete interface peaks and align these traces based on this reflection, as illustrated in Fig. 6. It is then a simple matter to determine the asphalt thickness since the asphalt surface reflection is well-defined and the asphalt-concrete reflection is usually easily detected. The next step is to locate the reflection peak from the top layer of reinforcement which is now simplified as compared to Fig. 5, since alignment of the concrete surface reflections tends to align the rebar reflections. The cover over reinforcement can now be determined since both the concrete and the rebar reflections are available.

Thresholding

In order to obtain a more reliable indication of the membrane-concrete interface and the layers of rebars, a new technique has been developed. It is known that the surface reflection from the asphalt, and the reflections from the asphalt-concrete interface and the rebars should all have the same positive polarity. Consequently, it is expected that significant information can be obtained by implementing a zero volt threshold which presents only positive data as expressed by the relation

$$r_T(t) = r(t) \quad ; \quad r(t) \geq 0V$$
$$= 0V \quad ; \quad r(t) < 0V$$

Figure 7 shows the results of thresholding applied to the waterfall plot of Fig. 6. Identification of the asphalt-concrete interface, the top layer of reinforcement and bottom layers of reinforcement become much more obvious since the extraneous reflection peaks are eliminated.

Strata plots

Visualize the bridge deck as being composed of strata with the asphalt as the first layer, the concrete cover over the reinforcement as the second layer, the top layer of reinforcement being the third layer and so on. The peaks of Fig. 7 are plotted as asterisks in Fig. 8 where it is seen that not only are the main boundaries clearly defined, but also other layers such as the layers of asphalt and the different layers of reinforcement are delineated.

Waterfall Plot Differencing

It has been demonstrated that for a bridge deck in sound condition, the data usually demonstrate very good consistency in the overall waveform signature, i.e. consecutive waveforms are almost replicas

of each other, as shown in Fig. 9. Conversely, for a bridge deck in poor condition, the radar signatures vary considerably from one waveform to another. It is noted that delamination can be identified by: first, aligning all the radar waveforms with respect to the reflection peak from concrete surface; and second, comparing changes in the pulse shape at the concrete surface peak. The 7 ns time mark is arbitrarily selected as the reference point for the concrete surface echo. Comparing with the waveform from good concrete, there are several features of the reflection peak from the concrete surface that are found to be associated with delamination. These include: 1) the trailing slope is less negative (Fig. 10a); and, 2) the pulsewidth is wider (Fig. 10b).

Initially, the reflection peaks from the concrete surface must be accurately aligned. The advantage of lining up the waveforms with respect to the concrete surface provides a good visual effect for discriminating good waveforms from distorted waveforms. For a bridge deck in very good condition, the set of waveforms shown in the waterfall plot are very similar to each other. If the consecutive waveform subtraction procedure is applied to the data set, the magnitude of the residue waveform is close to zero. Conversely, due to the difference in pulse shape, waveform subtraction between good and distorted waveforms will yield a non-zero residue. The same analogy can also be applied to waveform subtraction among distorted waveforms, since distorted waveforms usually have different pulse shapes.

Sample plots are given in Figs. 11, 12(a) and 12(b) to demonstrate the waveform differencing technique. It is noted that different amplitudes among waveforms with similar pulse shape also increase the magnitude of the residue waveform. In order to reduce this secondary effect, all waveforms are normalized with respect to the reflection peak from the concrete surface. The subtraction of waveforms in Fig. 11 yields very low residues which means that the concrete around the area is in good condition. The residue waveforms in Figs. 12a and b show considerable activity which indicates damaged concrete.

One of the most effective methods in assessing the results of waveform subtraction is to measure the root-mean-square (rms) values of the residue waveforms. Assume the normalized reflected radar waveform for the i th trace is $\mathbf{r_i(n)}$, each trace has N sample points, where $1 \le n \le N$. Then, the difference between the i th and the (i-1) th consecutive waveform is just

$$\Delta r_i(n) = r_i(n) - r_{i-1}(n) \tag{4}$$

Then, the rms value of $\mathbf{\Delta r_i(n)}$ is given by

$$r_{rms} = \sqrt{\frac{1}{(q-p)} \sum_{n=p}^{q} \Delta r_i^2(n)} \tag{5}$$

The parameters p and q are the minimum and maximum locations of the zero-crossing points bounded by the leading and trailing slopes of the reflection peaks, respectively, at the concrete surface of the two consecutive waveforms described by (4).

CORRELATION

The correlation study involved 10 different bridge decks. The bridge deck selected here for illustrative purposes is the Glen Miller Road underpass located on Highway 401, near Trenton, Ontario, and is shown in the photograph of Fig. 13. The deck, 35.9 m in length, was constructed in 1956 and is a single span rigid frame with box beams. The reinforcing details are: 1) over the beams, #11 (30 mm) bars at 300 mm centres within 5 m from the abutment end and #11 bars at 300 mm centres in the rest of the span; 2) between beams, #6 (15 mm) longitudinal bars at 500 mm centres; and, 3) #6 (15 mm) transverse bars at 500 mm centres throughout.

A previous condition survey indicated the average asphalt thickness to be 112 mm with the minimum being 65 mm and the maximum being 145 mm. The cover to top steel averaged 59.3 mm from 7 core samples. The half-cell reading indicated that 10% of the deck area had levels more negative than -0.35V. It is generally accepted that if the potential is more negative than -0.35V, then there is a greater than 90% probability that reinforcing steel corrosion is occurring in that area at the time of measurement. The condition survey also showed the presence of mastic membrane waterproofing.

DART Survey Results

Figures 14(a) and 14(b) show photographs of the northbound curb lane looking north and the southbound curb lane looking north, respectively. In both photos, there appears to be considerable surface damage to the asphalt. It was decided to collect impulse radar data with DART along five lines spaced at 0.5 m intervals for each of the two curb lanes.

Two core samples were taken on the Northbound lane and one was taken on the Southbound lane (see Fig. 23). These core samples are depicted in the photographs of Fig. 15a, b and c and indicate good bonding at the asphalt/membrane/concrete interfaces. The asphalt thicknesses at core locations 1, 2 and 3 were found from the core samples to be 95 mm, 100 mm and 90 mm, respectively. The top transverse layer of steel was intersected by only the core sample at location 3 and the cover there was found to be 38 mm. This rebar was seen to be slightly rusted which is in agreement with the half-cell readings.

Figure 16a illustrates the radar waveforms from a section of good bridge deck located 12 m to 16 m along line 2. Figure 16b illustrates the radar waveforms from a section of damaged bridge deck located 24 m to 28 m along line 7. In each case, the data are taken at 100 mm intervals along the bridge deck. All waveforms in the plot are aligned using the concrete surface reflection peak, as indicated. The surface reflection is easily identified by the strong positive peak, as indicated in both figures. The asphalt thickness is measured by taking the time difference between the surface reflection and the concrete reflection and employing (3). The reflections from the top layer of reinforcement are identified and a line is drawn connecting the peaks, as illustrated. This leads to the determination of cover over reinforcement. The other layers of reinforcement and the bottom of deck are identified by the remaining peaks of the waveform.

Figure 17 demonstrates the strength of the threshold plot, obtained from the data of Fig. 16a, in which the asphalt surface reflection, the concrete surface reflection and the top layer of rebars are all prominently displayed. Figure 18 depicts the strata plot in which the peaks of Fig. 17 are selected. Figure 19 provides the results of waterfall plot differencing in which the consecutive waveforms of the data from line 2 are subtracted and the rms values at the concrete peak are plotted. It is seen here that the values are below 0.1V for most of the trace.

Figure 20 is the threshold plot obtained from the data of Fig. 16b and Fig. 21 depicts the related strata plot. Figure 22 provides the results of waterfall plot differencing in which the consecutive waveforms of the data from line 7 are subtracted and the rms values at the concrete peak are plotted. It is seen here that the values are below 0.1V for the first 15 m and the last 7 m of the trace. However, between 15 m and 27 m, the height of the trace is more than double indicating damage.

Table II provides the results of measuring the asphalt thickness (first entry) and the cover over top layer of reinforcement (second entry in brackets) with the line average being given at the bottom of each column. Table III furnishes the final results of concrete deterioration for each of the 10 lines as a percent of the total. Finally, a grid line map of the bridge deck is presented in Fig. 23 locating the areas of damage as indicated by the 'x' symbol.

Actual Survey Results

Figure 24 is a photographic record of the Northbound lane of the bridge deck looking south with the asphalt removed. Details of damaged locations are presented in Fig. 25a, b, c, and d. where it is seen that significant portions of the deck suffer from delamination. Cover over reinforcement was measured for lines 1 to 5 from 25 m to 30 m, at 1 m intervals, using a covermeter and the results are given in Table IV. The areas of delamination obtained by using the chain drag method are represented in Fig. 23 by the shaded areas.

Correlation

The asphalt thickness at core locations 1, 2 and 3 were found to be 95 mm, 100 mm and 90 mm, respectively while DART predicted 100 mm at all three locations. Concrete cover at core location 3 was found to be 38 mm and DART predicted 41 mm. Comparison indicates that the covermeter and the predictions of DART are within ± 9% (see Table V).

Comparison of the predictions of the DART and the actual damaged bridge deck for lines 1 to 10 is provided in Fig. 23. It is seen that there is good agreement except for the region between 30 m and 33 m on lines 7 to 9.

CONCLUSIONS

Impulse radar has certain advantages over the more conventional techniques in the evaluation of bridge decks including: 1) the method is non-destructive; 2) the data can be collected in a relatively short period of time; 3) the data can be collected for any desired portion of the deck in any desired detail; 4) the data can be easily stored by digital means for archival purposes; and 5) the procedure is more cost effective. However, the interpretation of the waveforms requires a considerable amount of effort since there are many different variables.

The enhancements in the data processing developed as part of this correlation study have considerably improved the accuracy of the DART surveys over the previous technique that relied on "Characteristic W". Further work is planned to overcome problems when the concrete cover to reinforcements is less than 25 mm and the delaminations are localized over the diameter of the reinforcement only.

REFERENCES

1. Manning, D. G., Barnes, D. F., Burkhardt, G. C., and Reel, R. S.: "Issues in Bridge Rehabilitation," Ministry of Transportation of Ontario, Report MAT-89-03, Downsview, Ontario, 1989.

2. Manning, D. G., and Holt, F. B. , "Detecting Deterioration in Asphalt-Covered Bridge Decks," Transport. Research Record 899, Washington, D.C., Jan. 1983, pp. 10-20.

3. Manning, D. G, and Masliwec A., "The Application of Radar and Thermography to Bridge Deck Condition Surveys", Research and Development Branch, Ministry of Transportation of Ontario, Report MAT-90-11, Downsview, Ontario, 1990.

4. Chung, T., Carter, C. R., Masliwec, A., and Manning, D. G., "Impulse Radar Evaluation of Asphalt-Covered Bridge Decks," IEEE Transactions on Aerospace and Electronic Systems, Vol. 28, No. 1, 1990, pp. 125-137.

5. Carter, C. R., Chung, T., Masliwec, A., and Manning, D. G., "Analysis of Radar Reflections from Asphalt Covered Bridge Deck Structures," in Ground Penetrating Radar, ed. J. Pilon; Geological Survey of Canada, Paper 90-4, 1992, pp. 33-40.

List of Tables

TABLE I : Overruns in 1986 Bridge Rehabilitation Contracts.

TABLE II : DART Survey
Asphalt thickness and Concrete cover thickness.

TABLE III: DART Survey
Bridge Deck Conditions.

TABLE IV : ACTUAL Survey
Covermeter Readings.

TABLE V : Concrete cover thickness comparison
Actual Survey vs. DART Survey.

List of Figures

Fig. 1: (a) DART van at bridge Deck.
(b) Detailed view of the radar system mounted on the front of the vehicle.

Fig. 2: Transmitted impulse radar waveform.

Fig. 3: Typical deck reinforcing details.

Fig. 4: (a) Model of a typical asphalt-covered bridge deck structure.
(b) Reflected waveform from a typical asphalt-covered bridge deck.

Fig. 5: Sample waterfall plot from a bridge deck. Note all the radar traces are aligned at the asphalt surface reflection peak.

Fig. 6: Sample waterfall plot with waveforms aligned at the concrete surface reflection peak.

Fig. 7: Sample thresholding plots using the set of data in Fig. 6.

Fig. 8: Sample strata plots using the set of data in Fig. 7.

Fig. 9: Sample radar traces from a section of good concrete section.

Fig. 10: (a) Sample radar traces from a section of delaminated concrete.
(b) Sample radar traces from a section of delaminated concrete.

Fig. 11: Waveform differencing between the two waveforms with similar pulse shape indicated by the symbol ' 'in Fig. 9. Note the magnitude of the residue waveform is close to zero.

Fig. 12: (a) Waveform differencing between the two waveforms with different pulse shape indicated by the symbol ' ' in Fig. 10 (a). Note the increase in the magnitude of the residue waveform.
(b) Waveform differencing between the two waveforms with different pulse shape indicated by the symbol ' ' in Fig. 10 (b). Note the increase in the magnitude of the residue waveform.

Fig. 13: Photograph of the bridge deck - Glen Miller Road Underpass/Hwy 401 with the elevation from east.

Fig. 14: (a) Northbound curb lane looking North. Note surface damage to the asphalt.
(b) Southbound curb lane looking North. Note surface damage to the asphalt.

Fig. 15: (a) Photograph of core sample #1 taken at 1 m from the west curb and 8.6 m from the north end joint.

Fig. 16: (a) Radar waveforms from a section of sound concrete along line 2 of the data set.
(b) Radar waveforms from a section of delaminated concrete, indicated by the symbol '*', along line 7 of the data set.

Fig. 17: Thresholding plots of the set of waveforms given in Fig. 16(a).

Fig. 18: Strata plots of the set of waveforms given in Fig. 17.

Fig. 19: The magnitude plot of the rms values after waveform differencing along line 2.

Fig. 20: Thresholding plots of set of waveforms given in Fig. 16(b).

Fig. 21: Strata plots of the set of waveforms given in Fig. 20.

Fig. 22: The magnitude plot of the rms values after waveform differencing along line 7.

Fig. 23: Grid line map of the bridge deck indicating areas of delaminations as predicted by DART survey (symbol 'x') and actual survey (shaded area). Note the locations of the three core samples are marked on the map.

Fig. 24: Photograph of the exposed concrete deck (with asphalt cover removed) along the Northbound lane looking south.

Fig. 25: Photographs of the exposed concrete decks (looking south) along line 7.
(a) from 18 m to 22 m from the north end joint.
(b) from 22 m to 26 m from the north end joint.
(c) from 26 m to 28 m from the north end joint.
(d) from 33 m to 35 m from the north end joint.

TABLE I: Overruns in 1986 Bridge Rehabilitation Contracts.

Region	Tender	As Constr.	Percent Overrun	Tendered Crew Hours	As Constr. Crew Hours	Percent Overrun
Southwest	4,441,349	4,867,350	9.6	112,915	156,916	39.0
Central	16,423,194	18,986,113	15.6	683,478	2,059,352	201.3
Eastern	5,872,195	6,118,025	4.2	275,832	306,249	11.0
North	5,232,556	5,835,409	11.5	65,745	126,712	92.7
Northwest	3,673,831	3,915,587	6.6	202,575	143,990	-28.9
TOTAL	35,643,050	39,722,484	11.4	1,340,545	2,793,218	103.4

TABLE II: DART Survey
Asphalt thickness and Concrete cover thickness.

-*-*-*- [SUMMARY: thicknesses] -*-*-*-

Site 11-186, Glen Miller Road Underpass/Hwy 401

LINE#	1	2	3	4	5	6	7	8	9	10
1m	98 (44)	83 (57)	78 (69)	83 (63)	84 (94)	112 (52)	111 (56)	104 (70)	92 (70)	80 (71)
2m	95 (46)	88 (54)	83 (60)	88 (66)	86 (78)	104 (50)	106 (53)	100 (56)	94 (58)	83 (61)
3m	93 (41)	90 (55)	90 (54)	100 (57)	103 (58)	112 (48)	116 (53)	113 (58)	102 (66)	87 (62)
4m	98 (38)	88 (53)	91 (55)	97 (64)	103 (62)	112 (50)	114 (60)	112 (60)	103 (47)	100 (47)
5m	92 (45)	90 (52)	87 (53)	95 (66)	99 (61)	105 (47)	107 (56)	107 (56)	99 (60)	98 (47)
6m	93 (44)	90 (53)	85 (59)	90 (66)	94 (62)	102 (45)	103 (57)	100 (63)	95 (57)	89 (52)
7m	92 (44)	92 (54)	84 (54)	88 (62)	93 (62)	98 (47)	100 (57)	98 (59)	96 (64)	87 (57)
8m	93 (45)	96 (55)	85 (62)	89 (60)	93 (55)	100 (48)	102 (51)	101 (55)	99 (62)	82 (57)
9m	112 (47)	98 (53)	87 (63)	93 (57)	94 (54)	94 (52)	95 (51)	96 (51)	95 (62)	92 (54)
10m	108 (44)	98 (58)	87 (57)	96 (49)	95 (48)	94 (59)	94 (46)	97 (55)	102 (58)	89 (73)
11m	104 (43)	98 (51)	89 (52)	93 (58)	94 (53)	93 (51)	95 (45)	95 (49)	99 (61)	110 (59)
12m	90 (44)	96 (51)	89 (54)	94 (66)	96 (55)	93 (50)	90 (55)	90 (56)	98 (54)	100 (66)
13m	109 (56)	100 (57)	91 (63)	96 (53)	96 (56)	95 (44)	94 (52)	95 (56)	94 (52)	97 (51)
14m	122 (46)	106 (51)	102 (57)	100 (53)	100 (50)	92 (48)	89 (59)	95 (56)	95 (46)	90 (69)
15m	109 (43)	104 (52)	105 (56)	101 (56)	101 (51)	89 (57)	87 (68)	93 (65)	85 (63)	95 (51)
16m	115 (40)	103 (51)	102 (63)	101 (55)	102 (56)	85 (60)	84 (68)	91 (63)	84 (59)	90 (52)
17m	115 (41)	103 (50)	104 (60)	105 (52)	106 (51)	85 (46)	85 (52)	90 (63)	81 (63)	84 (62)
18m	107 (48)	105 (58)	103 (61)	102 (56)	103 (52)	83 (44)	80 (42)	84 (54)	82 (59)	72 (68)
19m	107 (56)	105 (56)	101 (70)	101 (65)	99 (53)	82 (46)	79 (60)	82 (62)	75 (54)	69 (70)
20m	104 (56)	105 (56)	102 (64)	100 (68)	98 (54)	82 (60)	75 (64)	75 (54)	70 (49)	65 (71)
21m	111 (54)	103 (58)	99 (67)	100 (63)	99 (57)	82 (62)	75 (46)	74 (47)	70 (46)	59 (58)
22m	112 (51)	106 (59)	104 (62)	101 (54)	103 (49)	83 (66)	79 (68)	77 (63)	72 (50)	71 (67)
23m	106 (54)	104 (61)	105 (59)	103 (49)	108 (44)	86 (66)	84 (62)	76 (48)	74 (42)	72 (51)
24m	105 (58)	100 (54)	104 (57)	100 (53)	104 (47)	88 (69)	88 (61)	81 (57)	78 (50)	77 (51)
25m	106 (57)	101 (59)	98 (62)	97 (59)	106 (46)	88 (62)	90 (56)	86 (61)	82 (50)	79 (44)
26m	107 (52)	103 (62)	94 (63)	95 (59)	101 (53)	89 (48)	91 (59)	87 (62)	83 (44)	80 (53)
27m	110 (49)	103 (81)	98 (78)	96 (59)	97 (51)	83 (54)	86 (59)	86 (58)	81 (60)	75 (64)
28m	101 (44)	101 (57)	96 (52)	96 (53)	96 (53)	83 (46)	91 (60)	86 (65)	84 (54)	82 (55)
29m	94 (43)	92 (60)	93 (73)	96 (55)	98 (54)	87 (61)	86 (74)	81 (68)	80 (50)	79 (56)
30m	91 (46)	90 (50)	91 (67)	94 (55)	95 (49)	85 (61)	85 (68)	78 (64)	78 (43)	73 (56)
31m	91 (47)	92 (50)	91 (55)	91 (54)	95 (49)	85 (61)	84 (69)	78 (72)	68 (45)	68 (66)
32m	89 (47)	93 (67)	89 (59)	90 (51)	91 (50)	84 (62)	80 (67)	73 (58)	65 (55)	63 (64)
33m	88 (45)	90 (69)	88 (69)	88 (43)	91 (55)	81 (66)	76 (73)	66 (58)	57 (63)	58 (56)
34m	84 (51)	89 (62)	87 (62)	87 (58)	92 (56)	80 (54)	79 (70)	71 (49)	62 (49)	57 (46)
35m	87 (65)	88 (65)	86 (74)	84 (60)	90 (51)	80 (51)	82 (61)	73 (55)	61 (40)	57 (41)
36m	87 (53)	85 (67)	84 (68)	84 (64)	87 (64)	83 (55)	82 (65)	76 (53)	67 (63)	60 (54)
37m	87 (47)	87 (56)	88 (58)	88 (66)	93 (56)	88 (59)	86 (56)	75 (57)	67 (37)	60 (41)
AVE	100 (48)	96 (57)	93 (61)	95 (58)	97 (55)	90 (54)	90 (59)	88 (58)	83 (54)	79 (57)

TABLE III: DART Survey Bridge Deck Conditions.

[CONDITIONS: PERCENT OF DAMAGE]

LINE#	1	2	3	4	5	6	7	8	9	10
SCALE	.00	.00	.00	.00	.00	.00	.00	.00	.00	2.46
DELAMINATION	.82	.55	.55	.00	.55	3.83	6.04	3.84	1.64	2.19
GOOD	99.18	99.45	99.45	100.00	99.45	96.17	93.96	96.16	98.36	95.36
TOTAL	100.00	100.00	100.00	100.00	100.00	100.00	100.00	100.00	100.00	100.00

TABLE IV: ACTUAL Survey
Covermeter Readings

COVERMETER READINGS (mm)
(Transverse bars)

LINE	1	2	3	4	5
25 m	62	76	76	65	52
26 m	60	64	85	55	46
27 m	75	73	76	71	49
28 m	75	76	76	76	57
29 m	75	60	62	62	65
30 m	70	50	53	65	81

TABLE V: Concrete cover thickness comparison
Actual Survey vs DART Survey.

CONCRETE COVER COMPARISON (%)
DART measurement vs Covermeter reading

LINE	1	2	3	4	5
25 m	±4.03	±11.18	±9.21	±4.62	±5.77
26 m	±6.67	±1.56	±12.94	±3.64	±7.61
27 m	±17.33	±4.94	±1.32	±8.45	±2.04
28 m	±20.67	±12.50	±15.79	±15.13	±3.50
29 m	±21.33	±0.00	±8.87	±5.65	±8.46
30 m	±17.14	±0.00	±13.21	±7.69	±19.75
AVE	±14.53	±5.03	±10.22	±7.53	±7.86
TOTAL AVERAGE		±9.03			

(a)

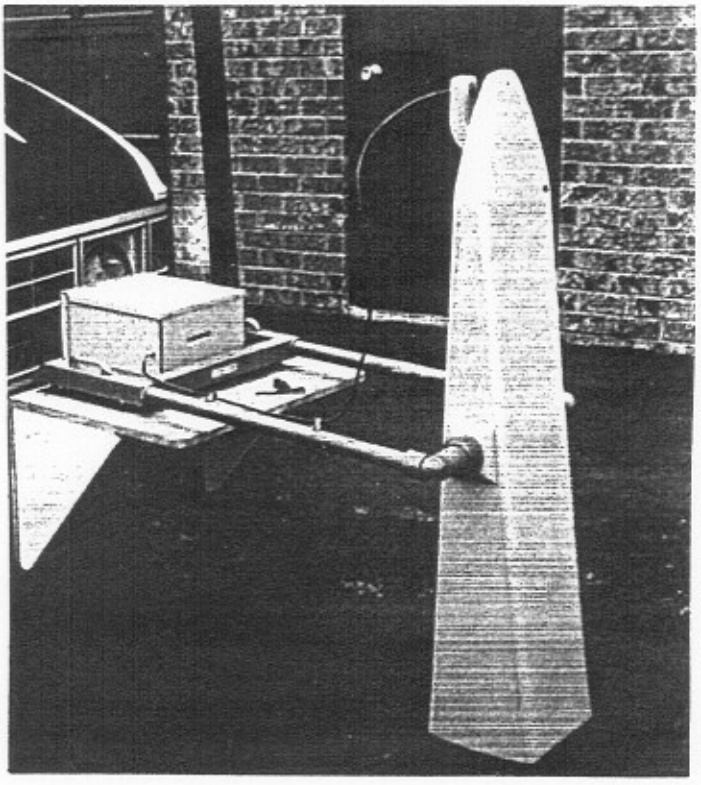

(b)

Fig. 1: (a) DART van at a bridge deck.
(b) Detailed view of the radar system mounted on the front of the vehicle.

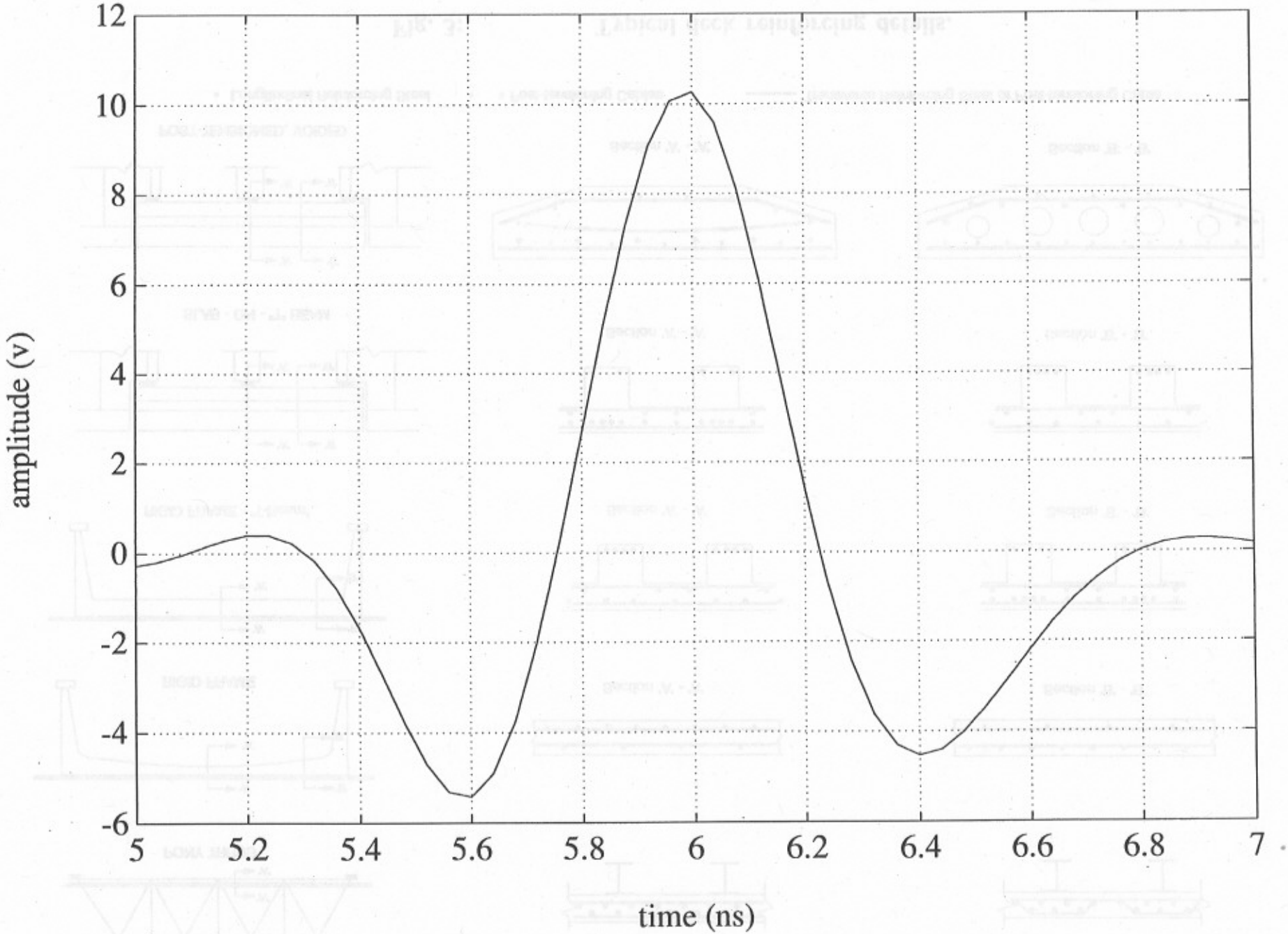

Fig. 2: **Transmitted impulse radar waveform.**

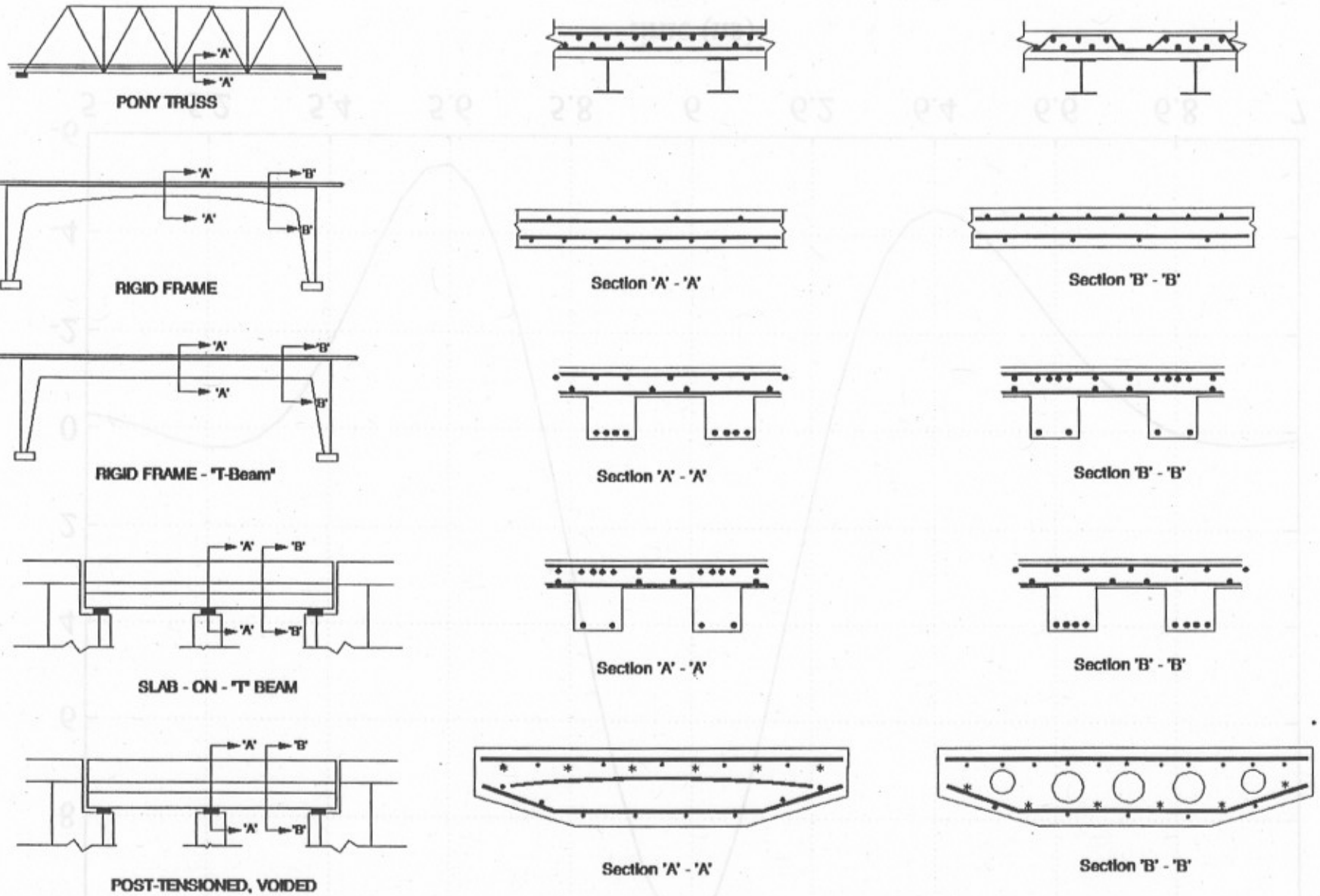

Fig. 3: Typical deck reinforcing details.

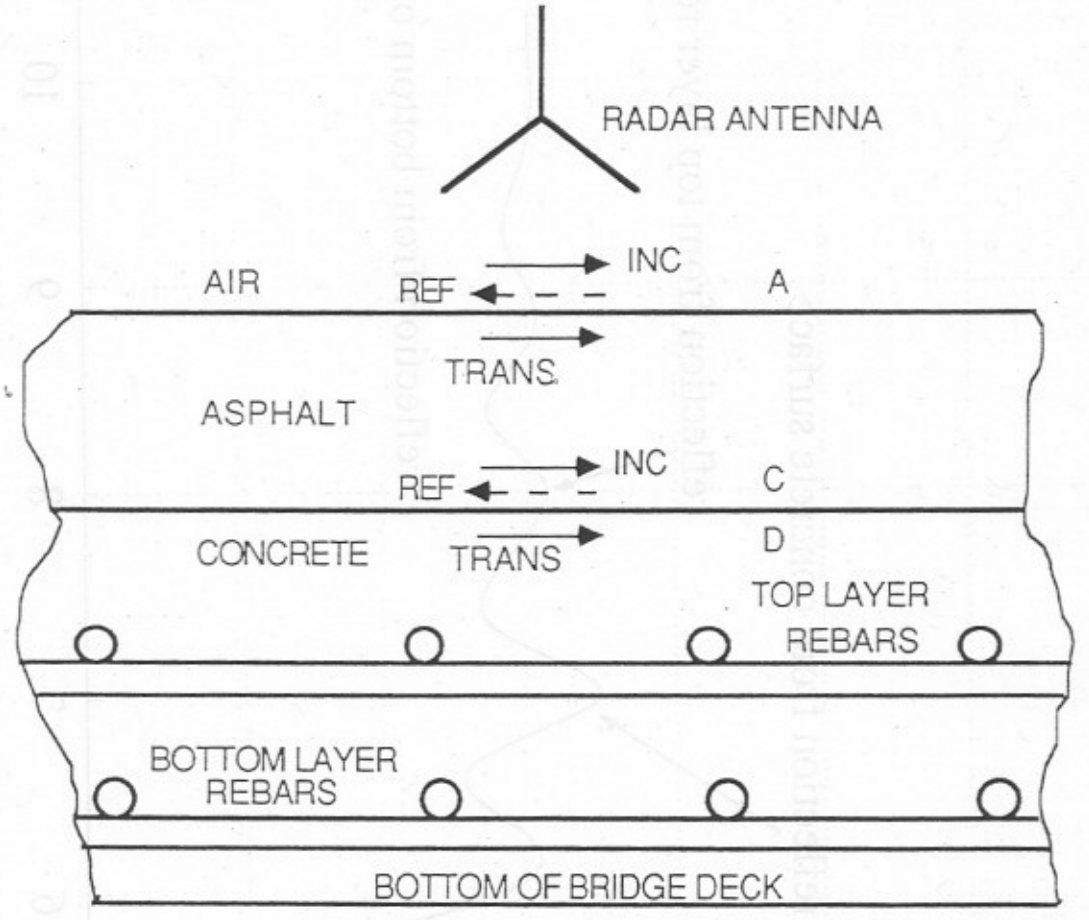

Fig. 4(a): Model of a typical asphalt-covered bridge deck structure.

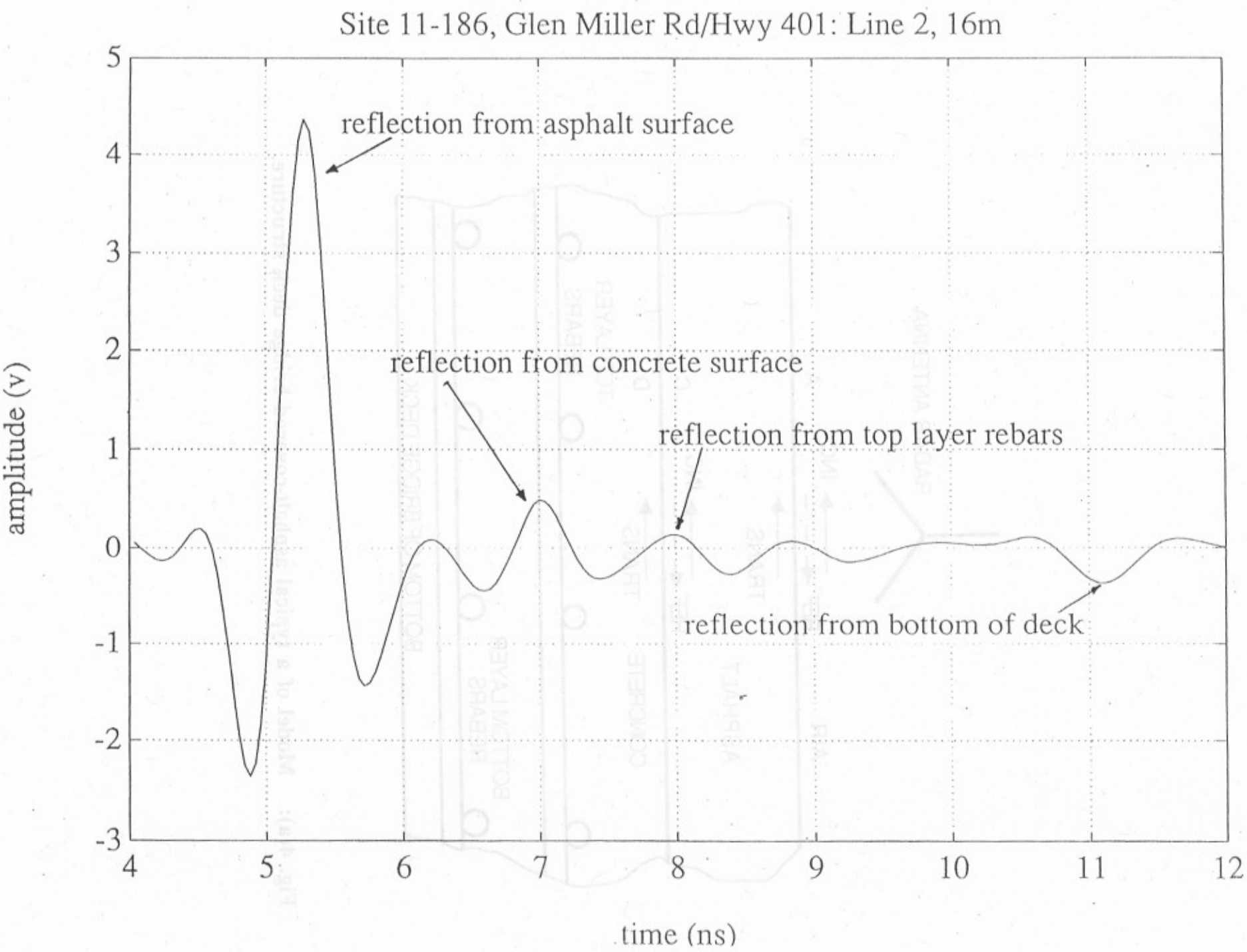

Fig. 4(b): Reflected waveform from a typical asphalt-covered bridge deck.

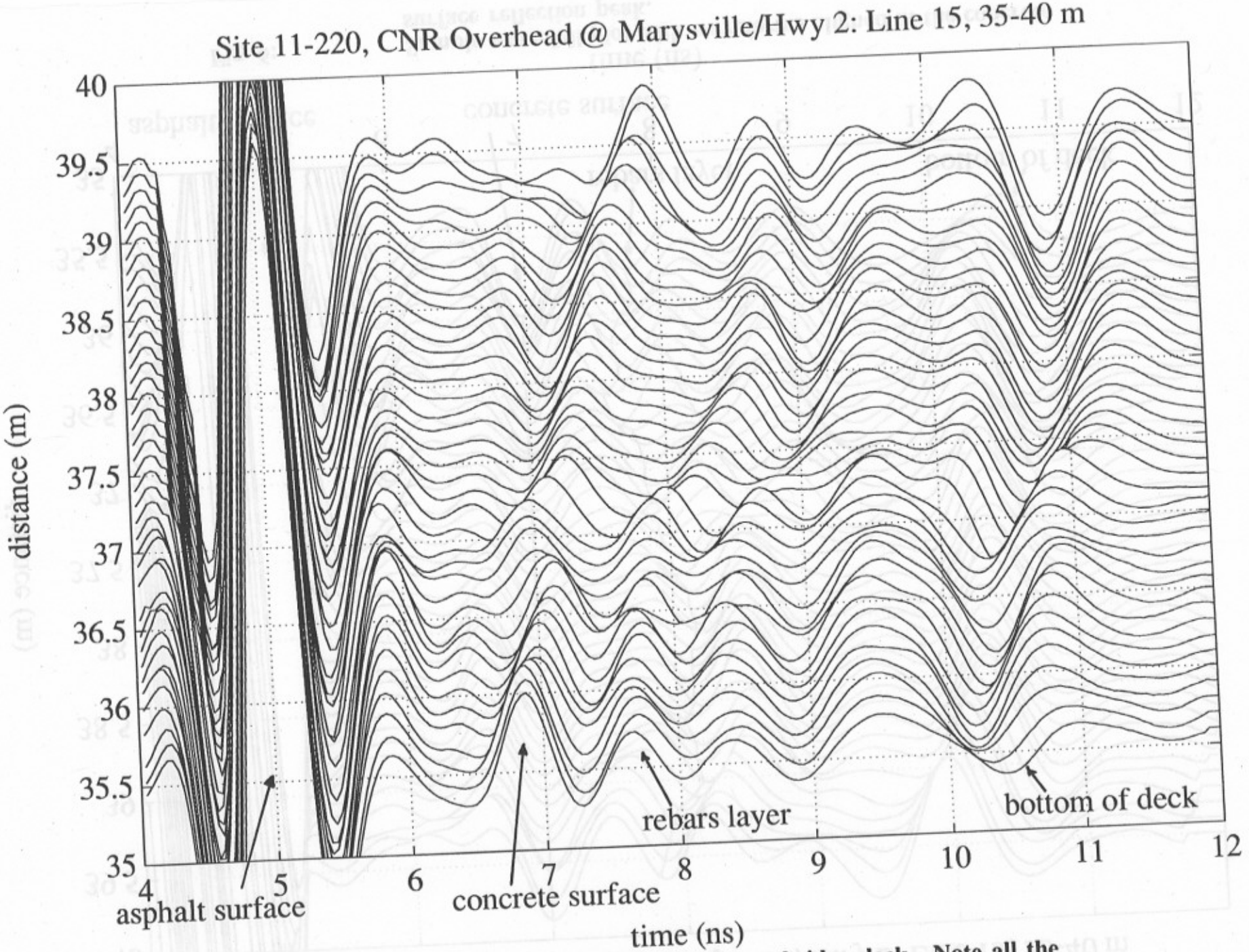

Fig. 5: **Sample waterfall plot from a bridge deck. Note all the radar traces are aligned at the asphalt surface reflection peak.**

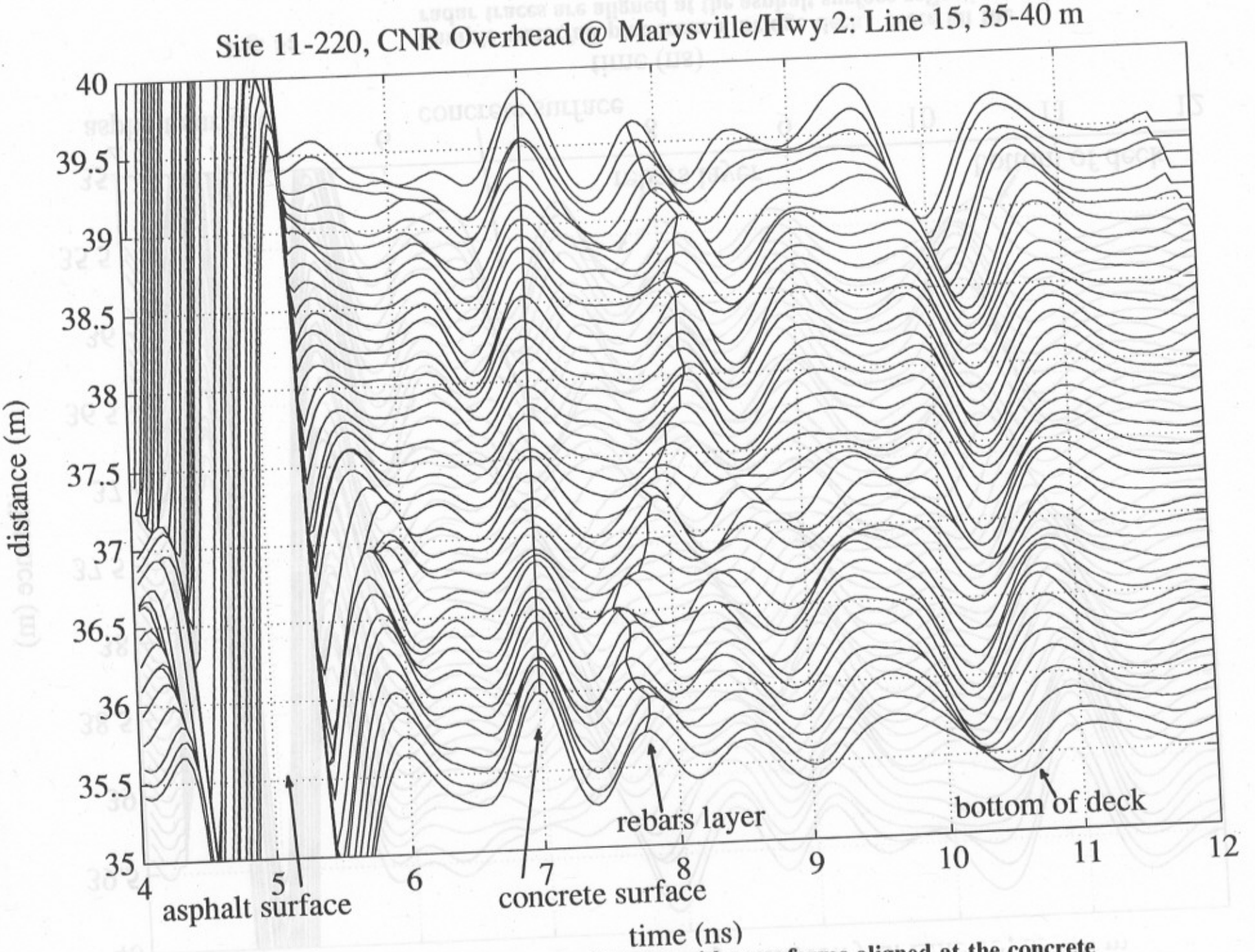

Fig. 6: **Sample waterfall plot with waveforms aligned at the concrete surface reflection peak.**

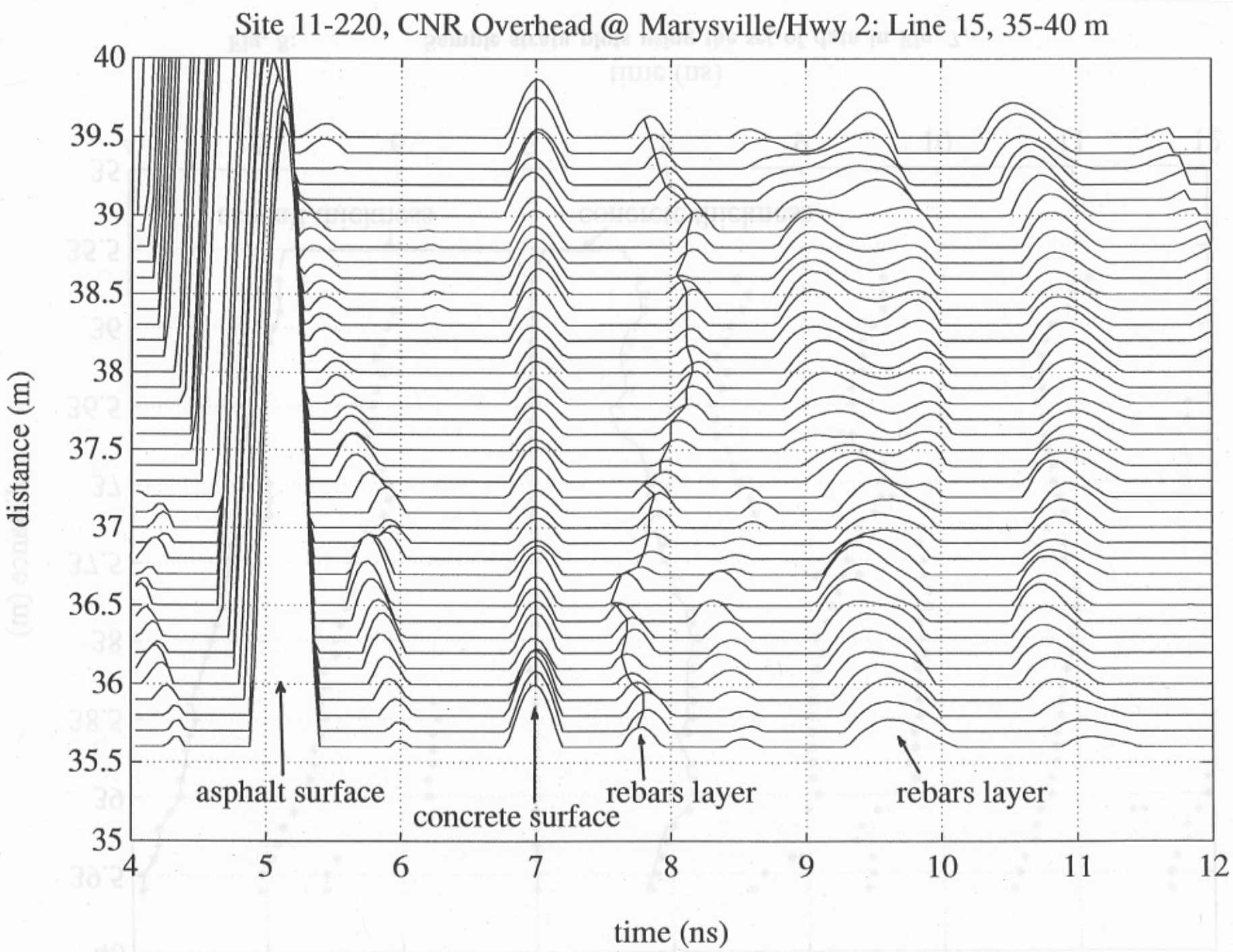

Fig. 7: **Sample thresholding plots using the set of data in Fig. 6 .**

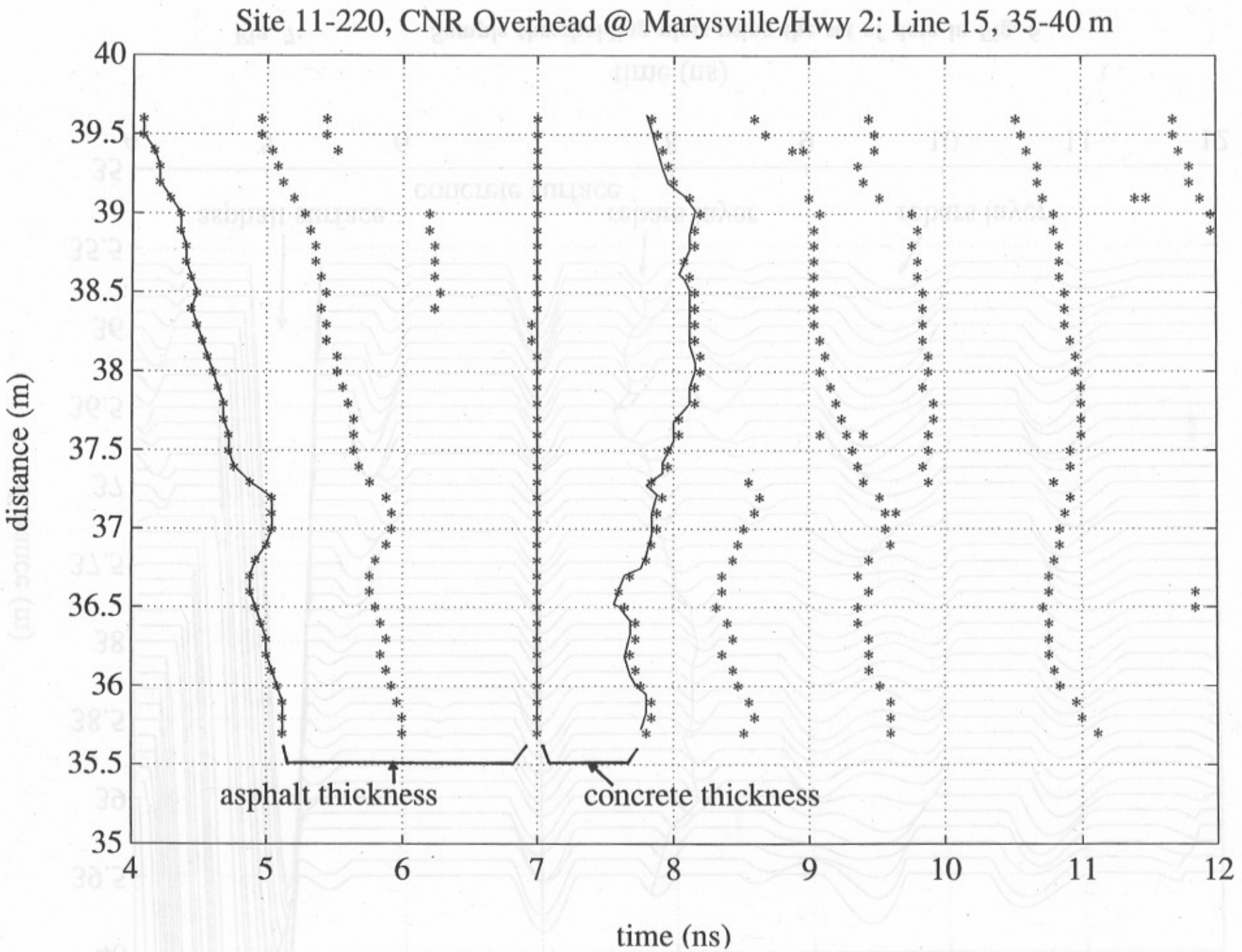

Fig. 8: **Sample strata plots using the set of data in Fig. 7.**

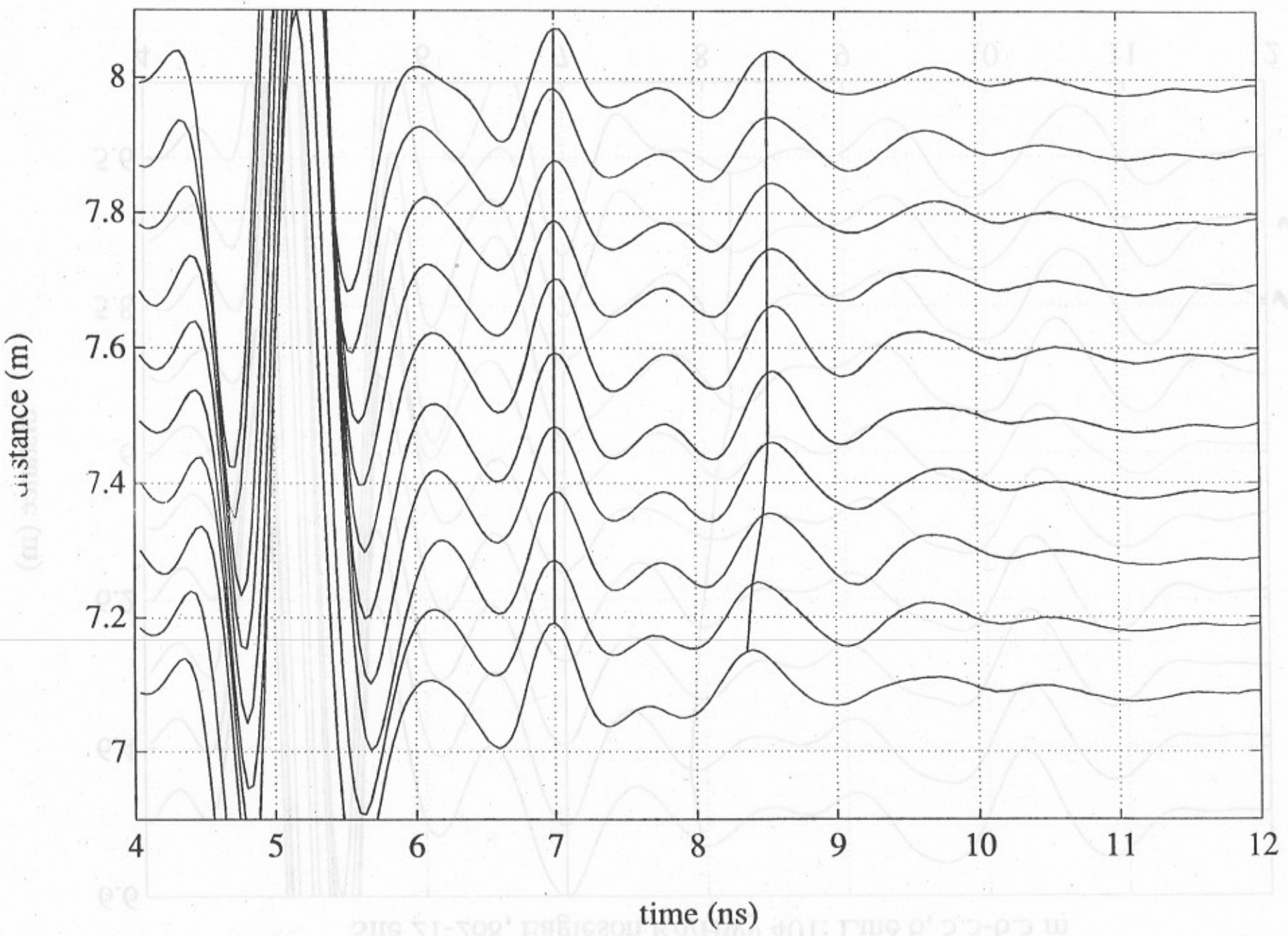

Fig. 9: **Sample radar traces from a section of good concrete.**

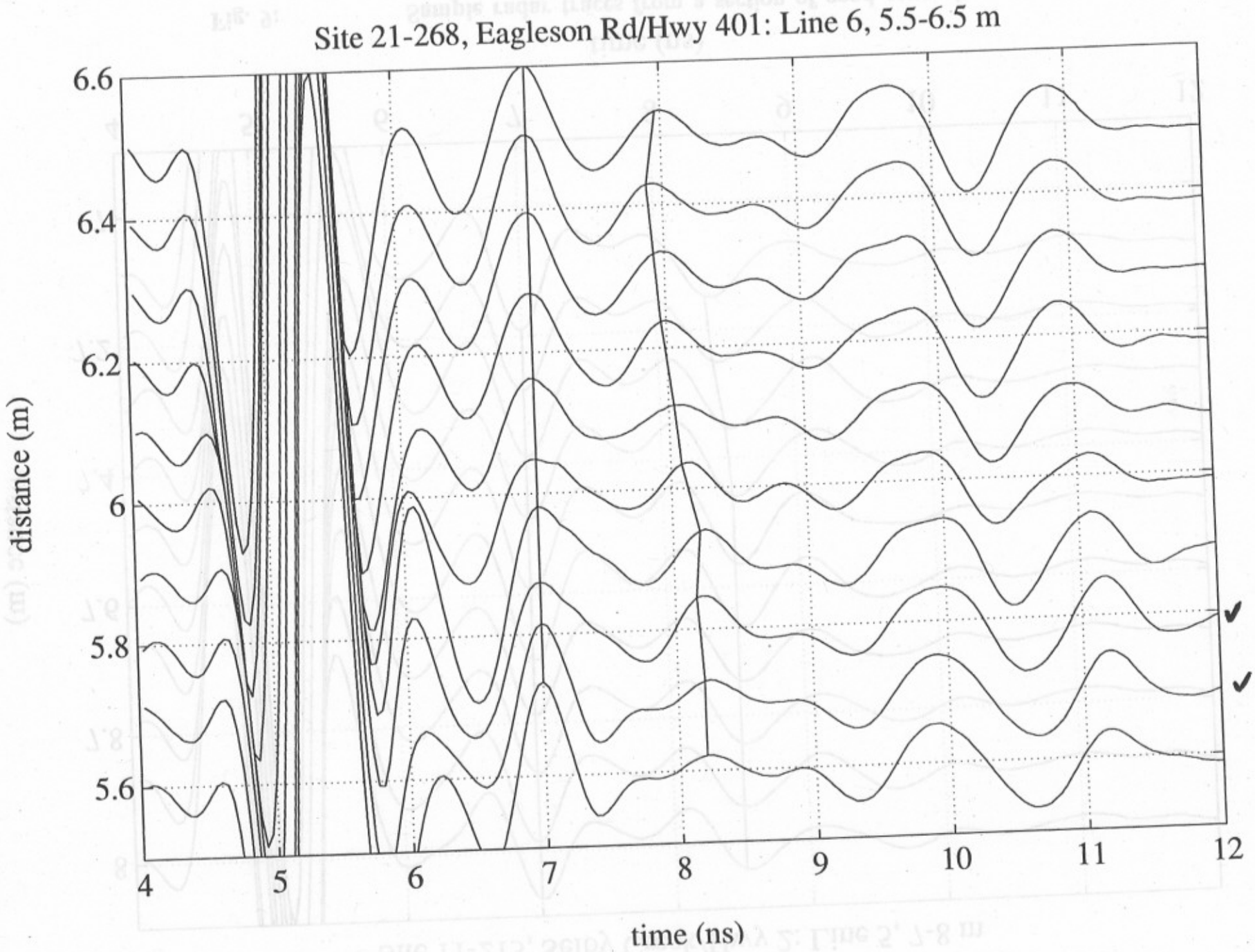

Fig. 10(a): Sample radar traces from a section of delaminated concrete.

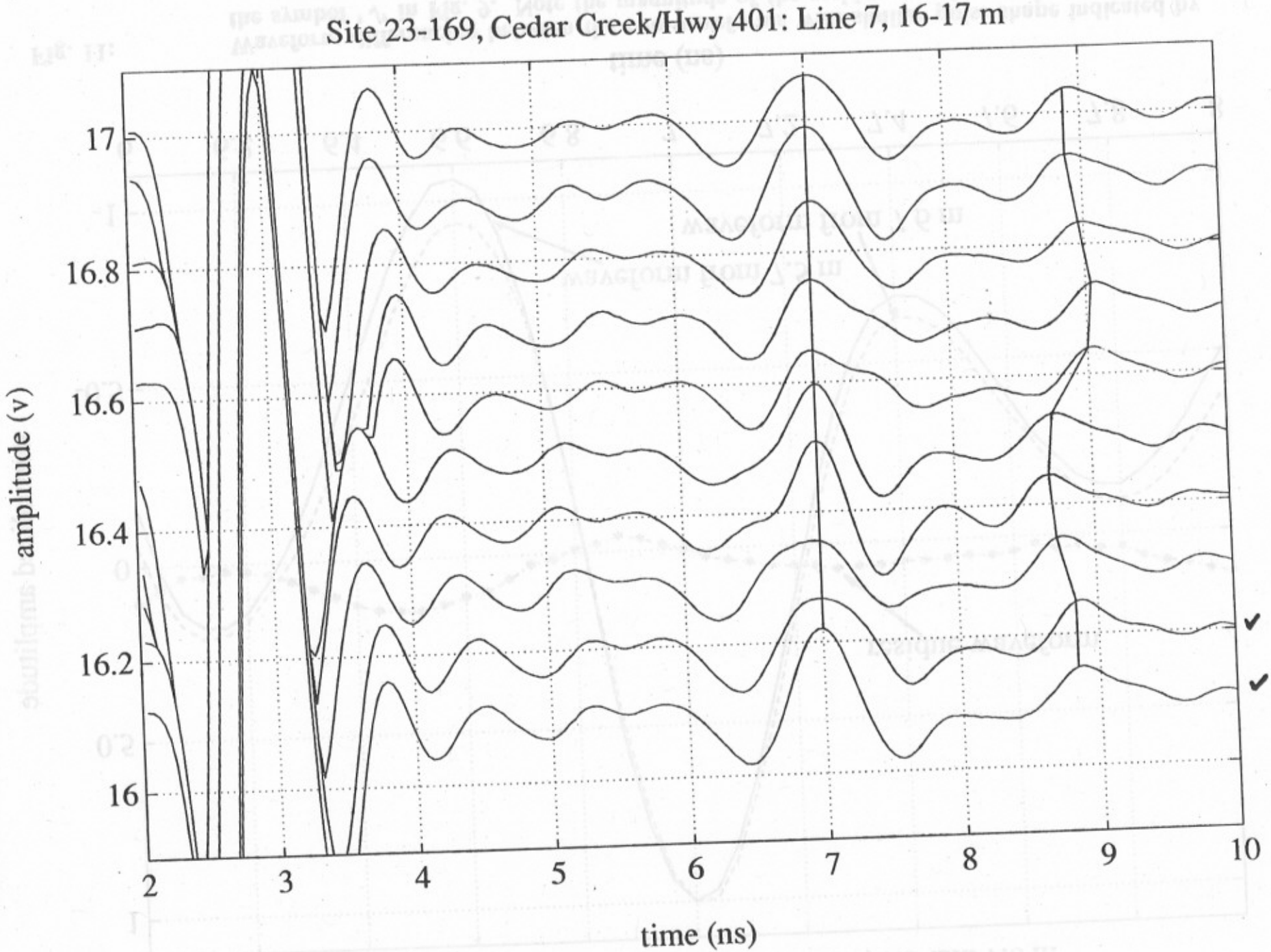

Fig. 10(b): Sample radar traces from a section of delaminated concrete.

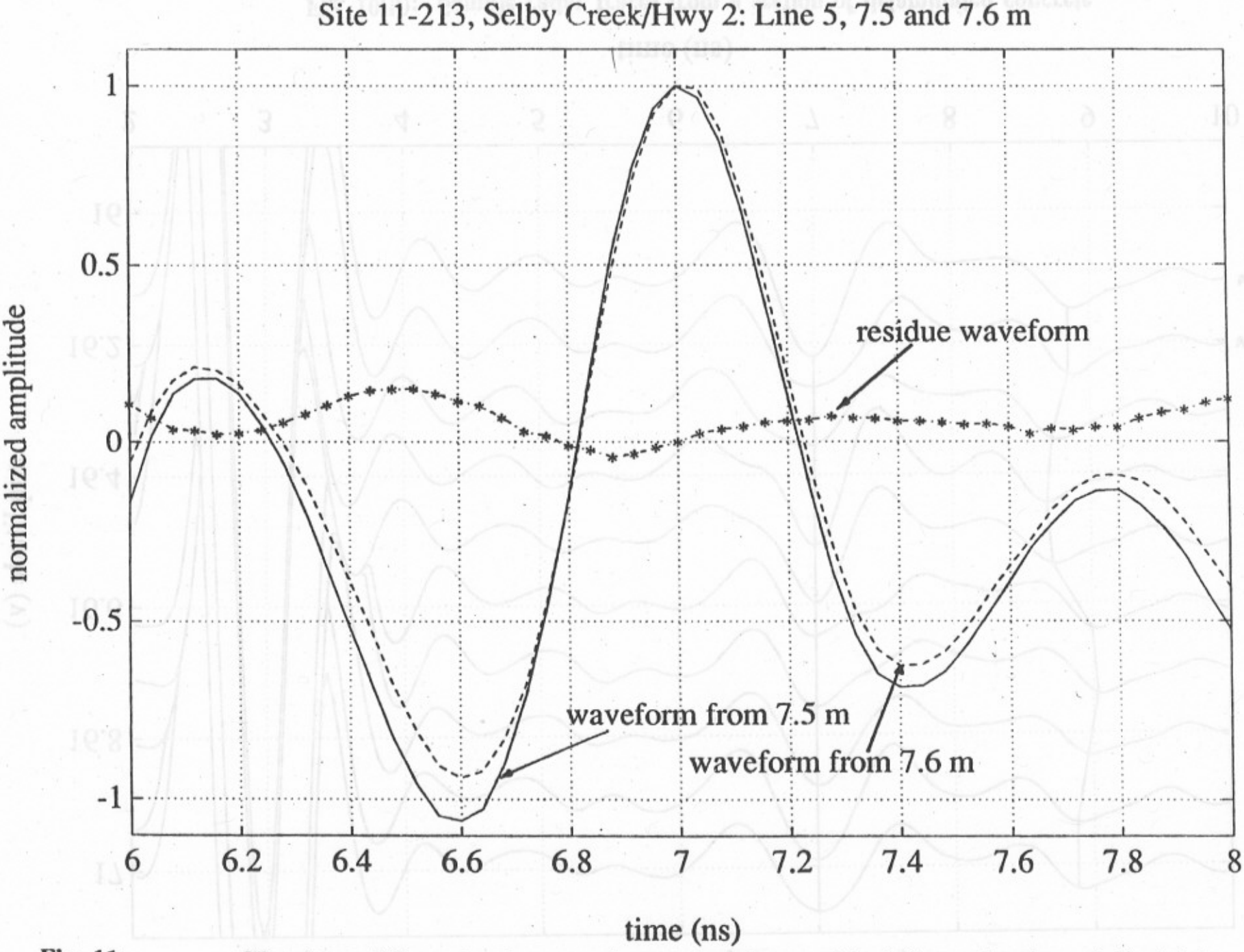

Fig. 11: **Waveform differencing between the two waveforms with similar pulse shape indicated by the symbol '√' in Fig. 9. Note the magnitude of the residue waveform is close to zero.**

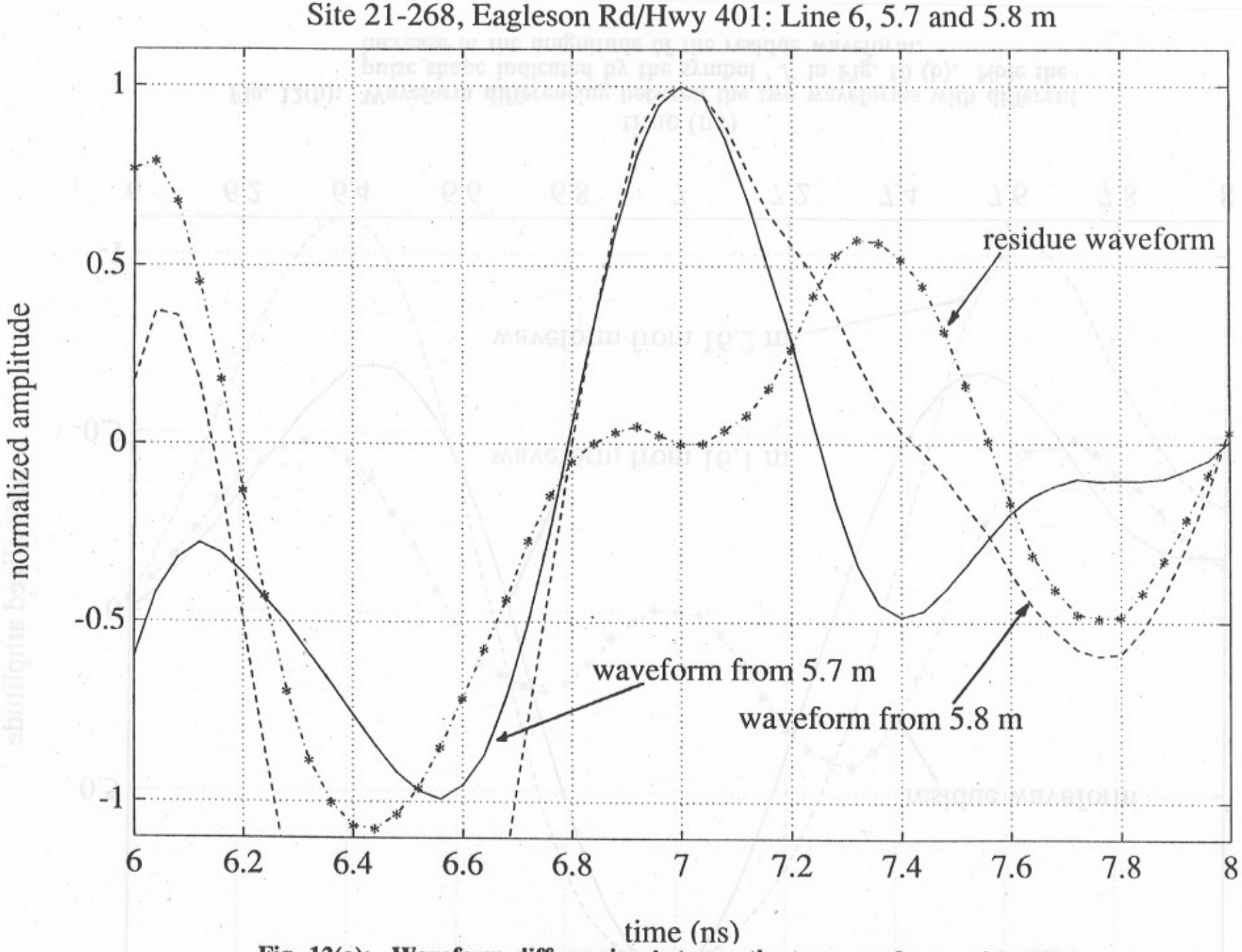

Fig. 12(a): Waveform differencing between the two waveforms with different pulse shape indicated by the symbol '√' in Fig. 10 (a). Note the increase in the magnitude of the residue waveform.

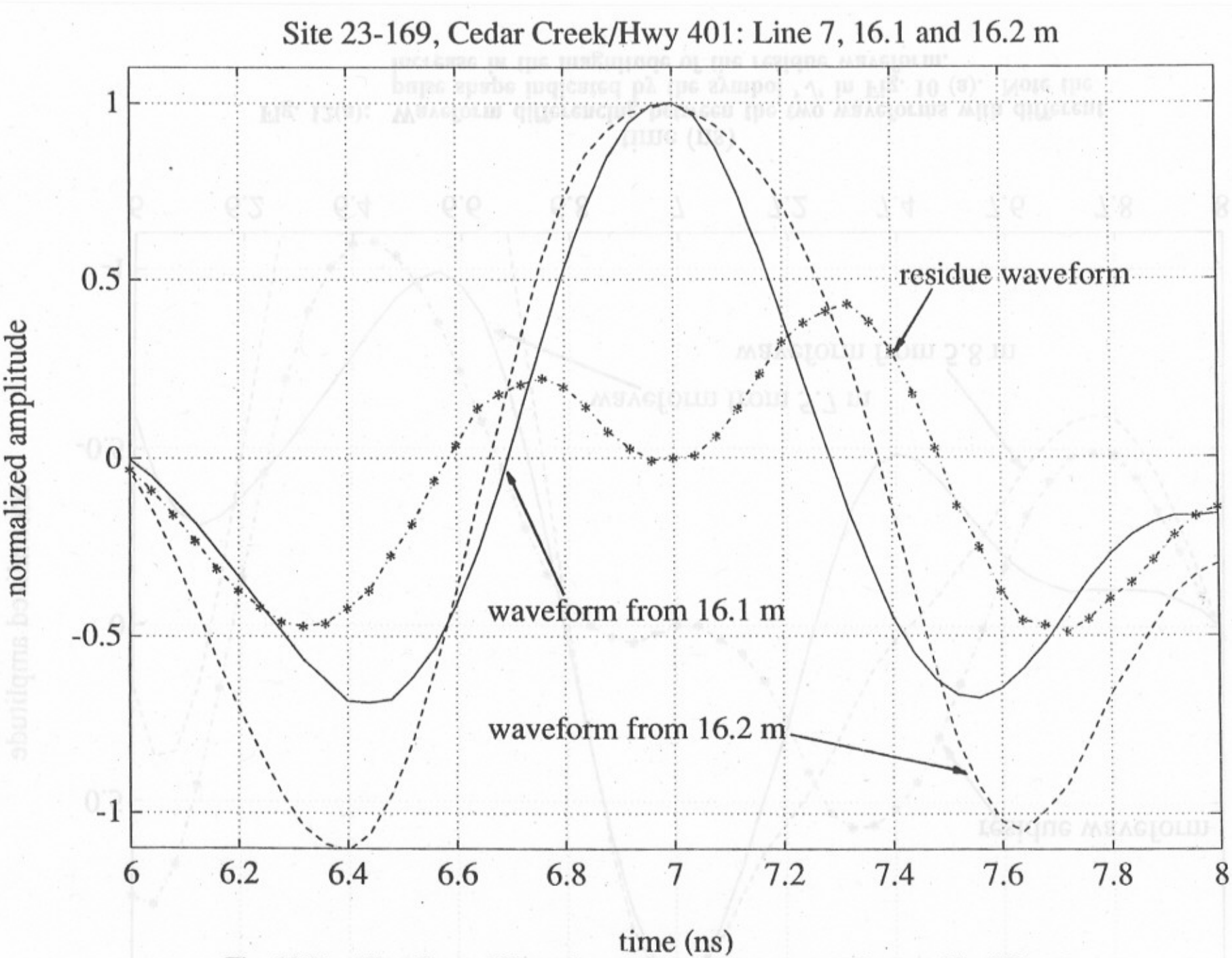

Fig. 12(b): Waveform differencing between the two waveforms with different pulse shape indicated by the symbol '√' in Fig. 10 (b). Note the increase in the magnitude of the residue waveform.

Fig. 13: **Photograph of the bridge deck - Glen Miller Road Underpass/Hwy 401 with the elevation from east.**

(b)

(a)

Fig. 14: (a) Northbound curb lane looking North.
(b) Southbound curb lane looking North.
Note surface damage to asphalt on both curb lanes.

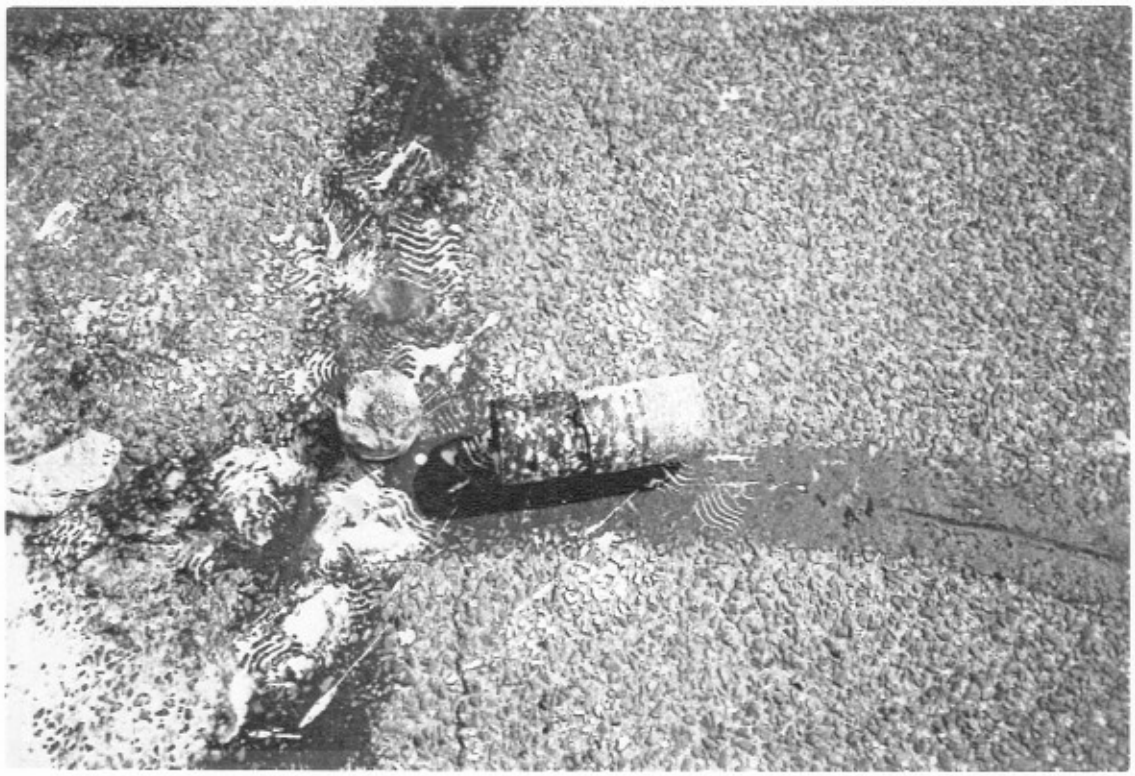

(a)

(b)

Fig. 15(a)-(b): (a) Photograph of core sample #1 taken at 1 m from the west curb and 8.6 m from the north end joint.

(b) Photograph of core sample #2 taken at 2 m from the west curb and 18.75 m from the north end joint.

Fig. 15(c): **Photograph of core sample #3 taken at 12 m from the west curb and 13.8 m from the north end joint.**

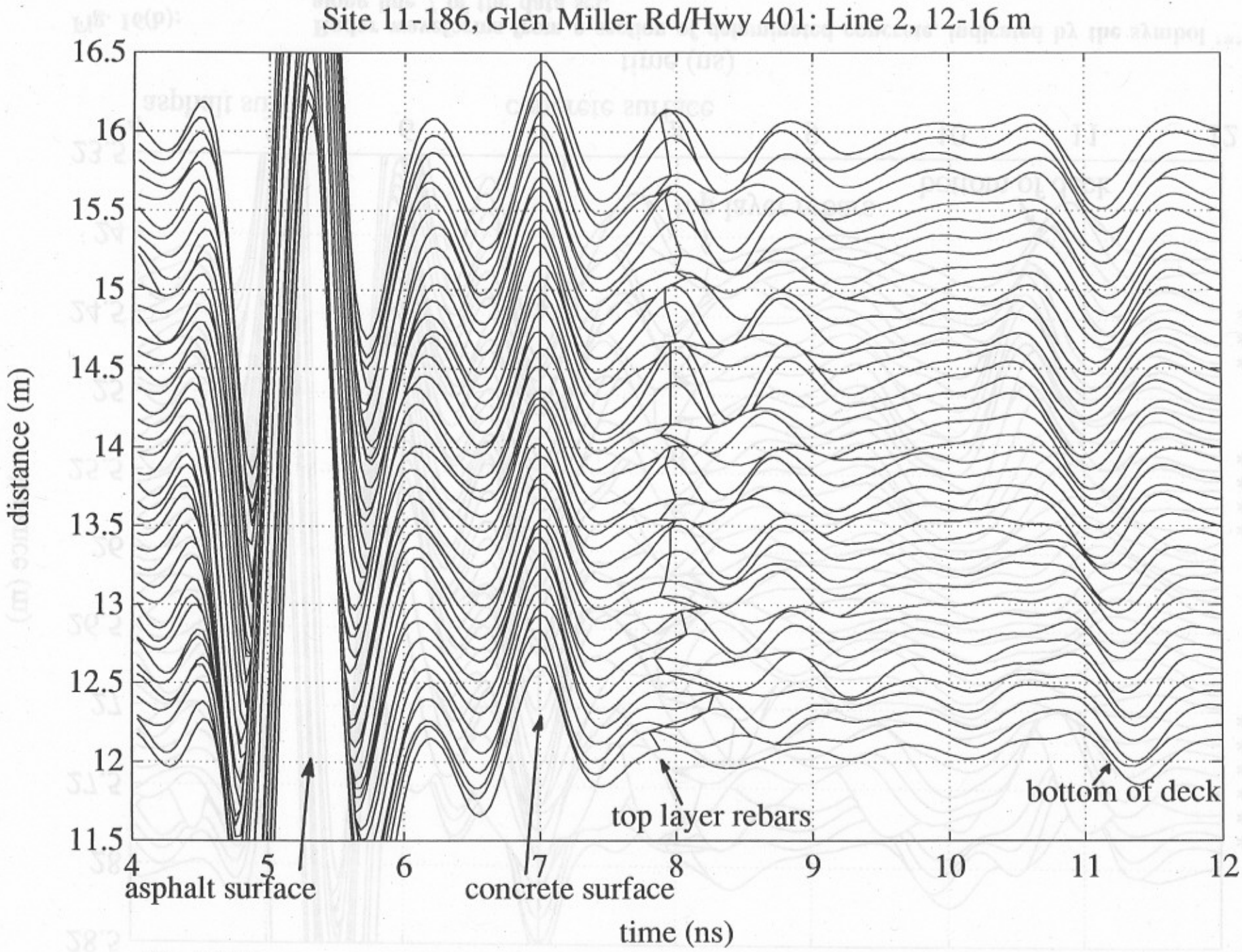

Fig. 16(a): **Radar waveforms from a section of sound concrete along line 2 of the data set.**

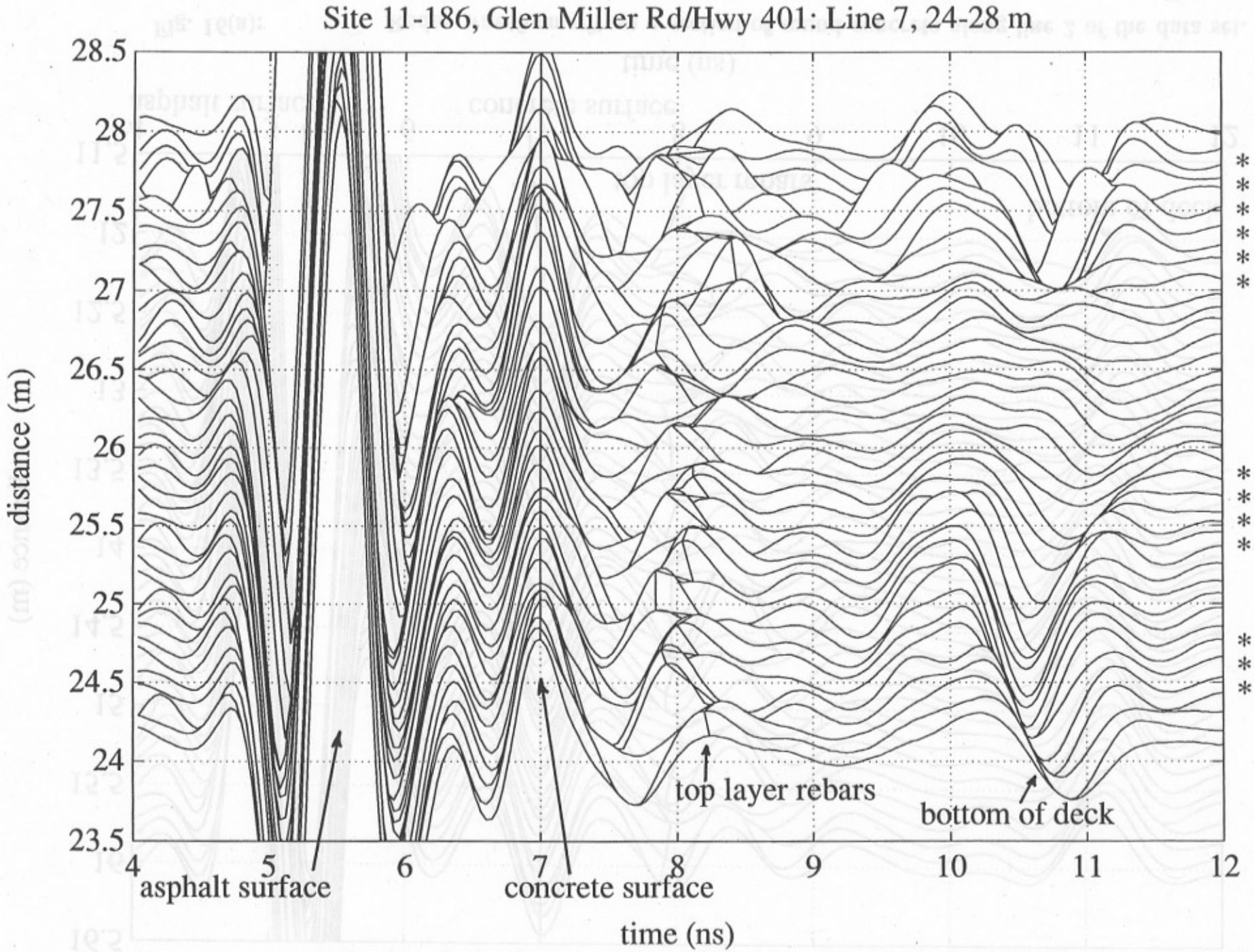

Fig. 16(b): **Radar waveforms from a section of delaminated concrete, indicated by the symbol '*', along line 7 of the data set.**

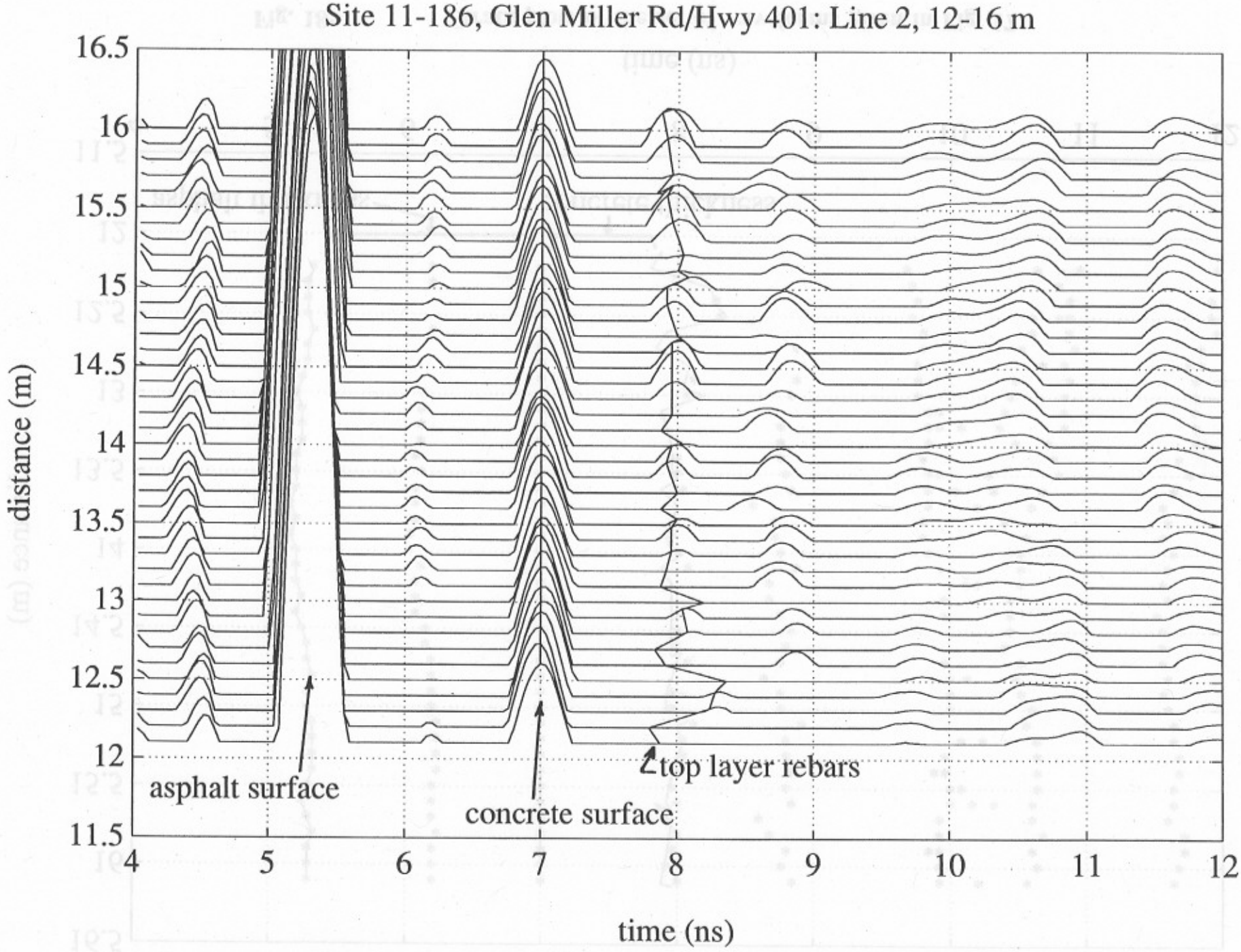

Fig. 17: **Thresholding plots of the set of waveforms given in Fig. 16(a).**

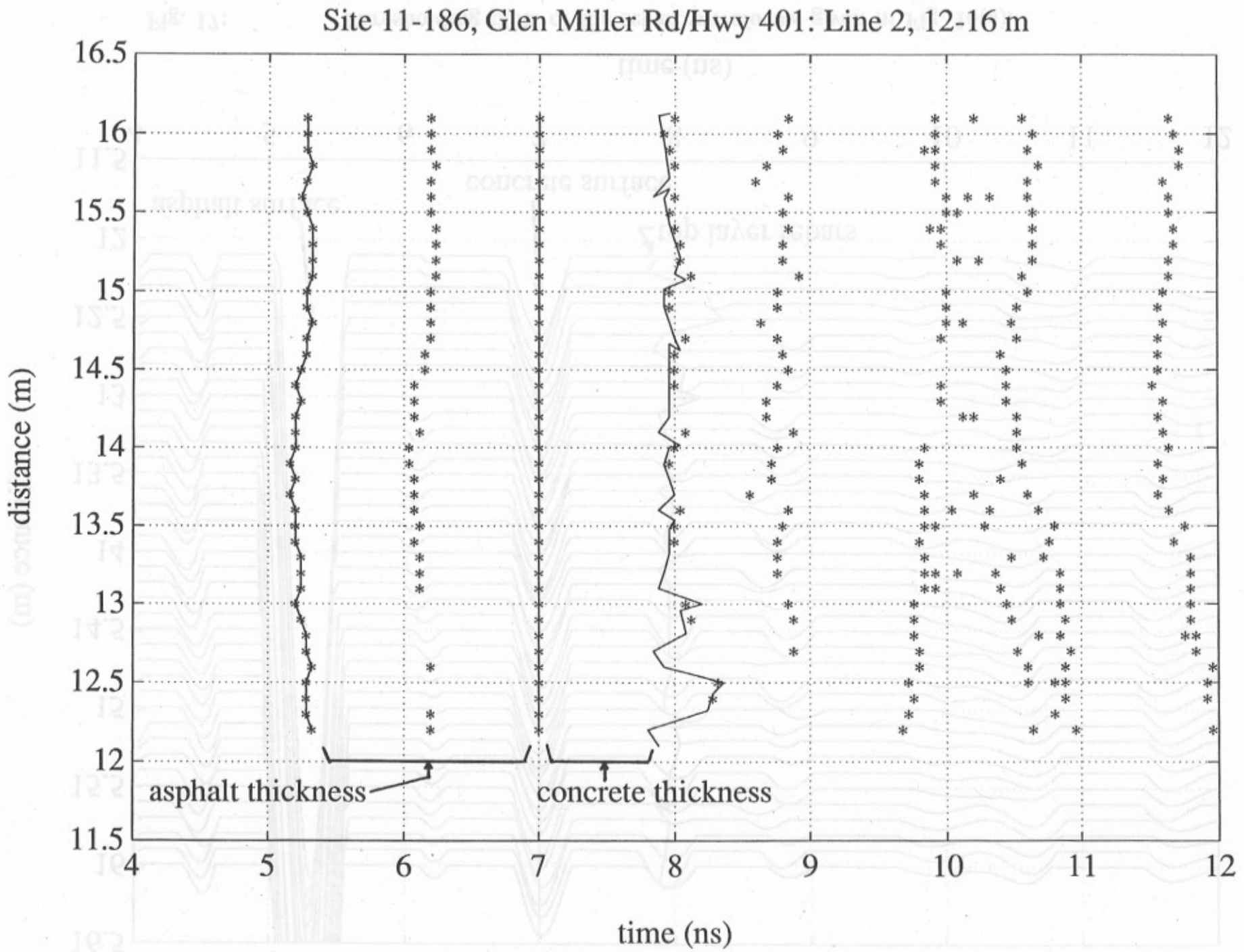

Fig. 18: **Strata plots of the set of waveforms given in Fig. 17.**

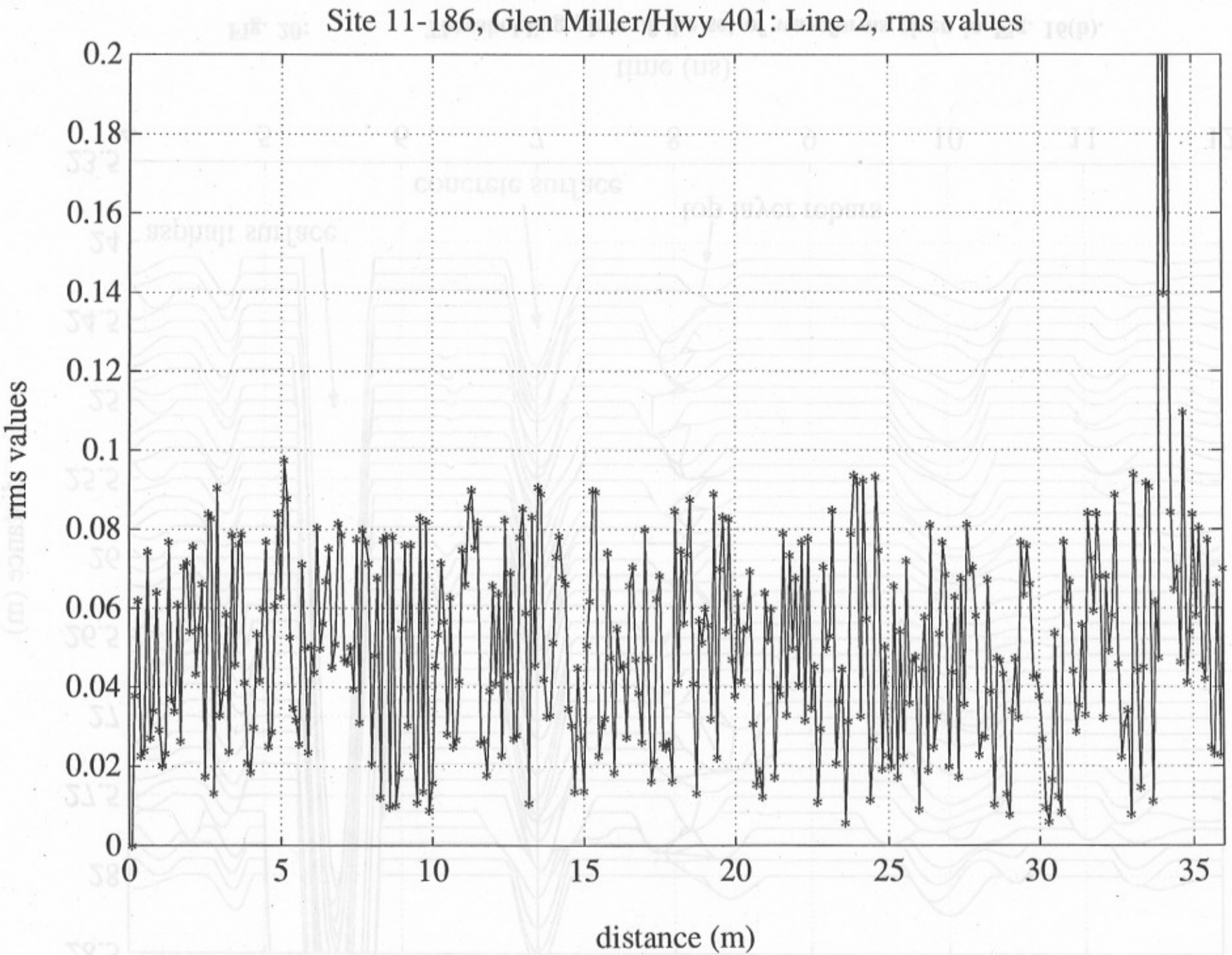

Fig. 19: **The magnitude plot of the rms values after waveform differencing along line 2.**

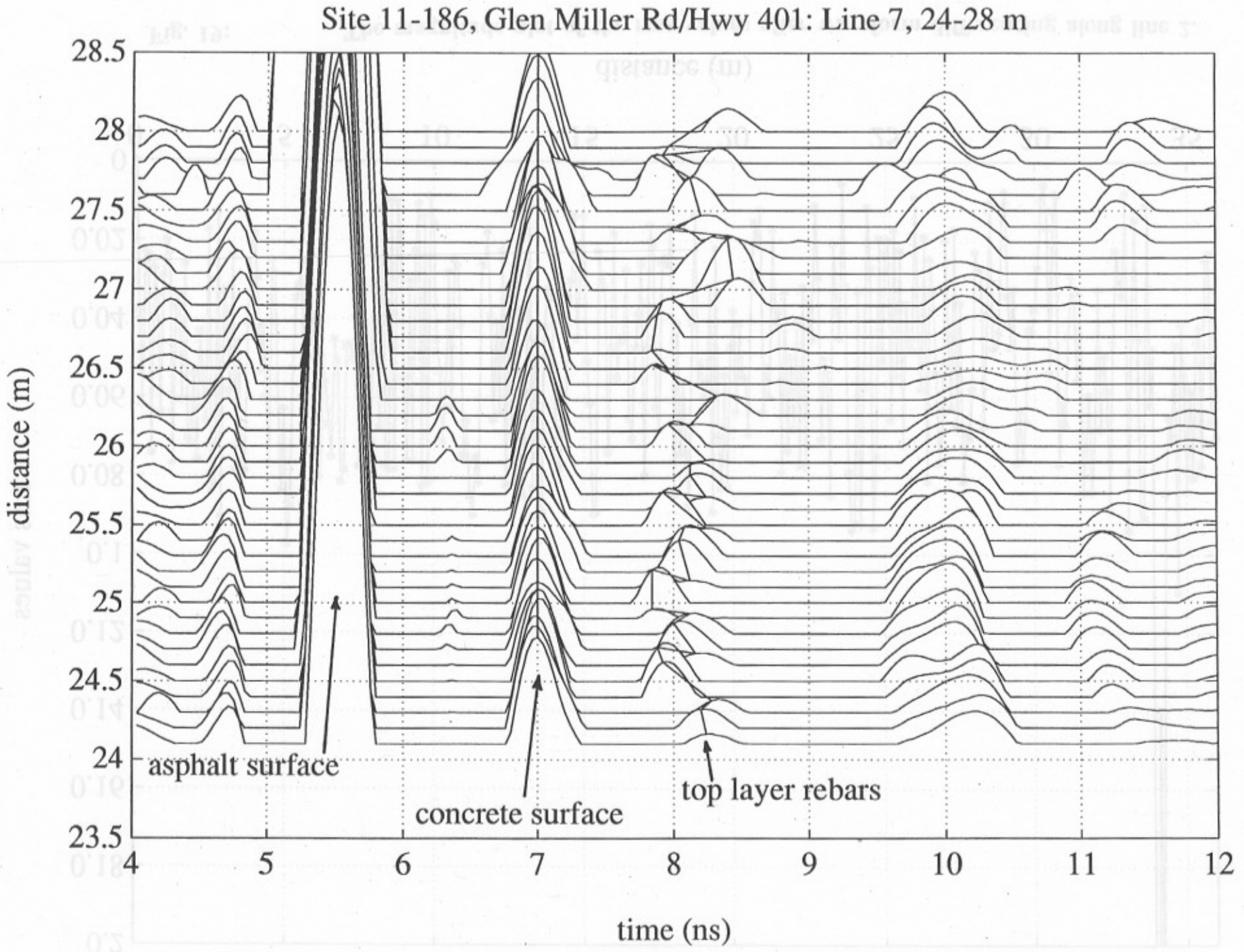

Fig. 20: **Thresholding plots of the set of waveforms given in Fig. 16(b).**

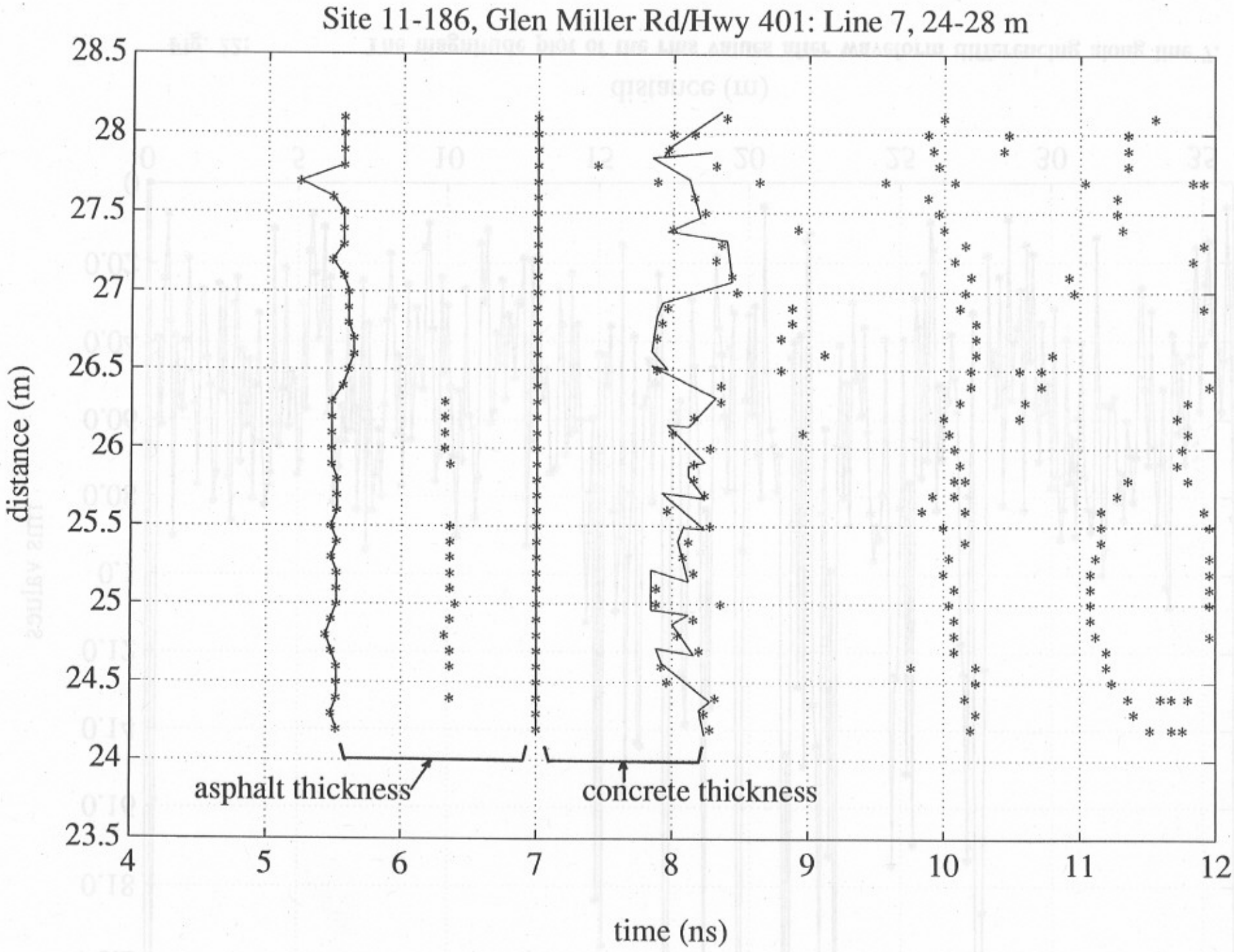

Fig. 21: **Strata plots of the set of waveforms given in Fig. 20.**

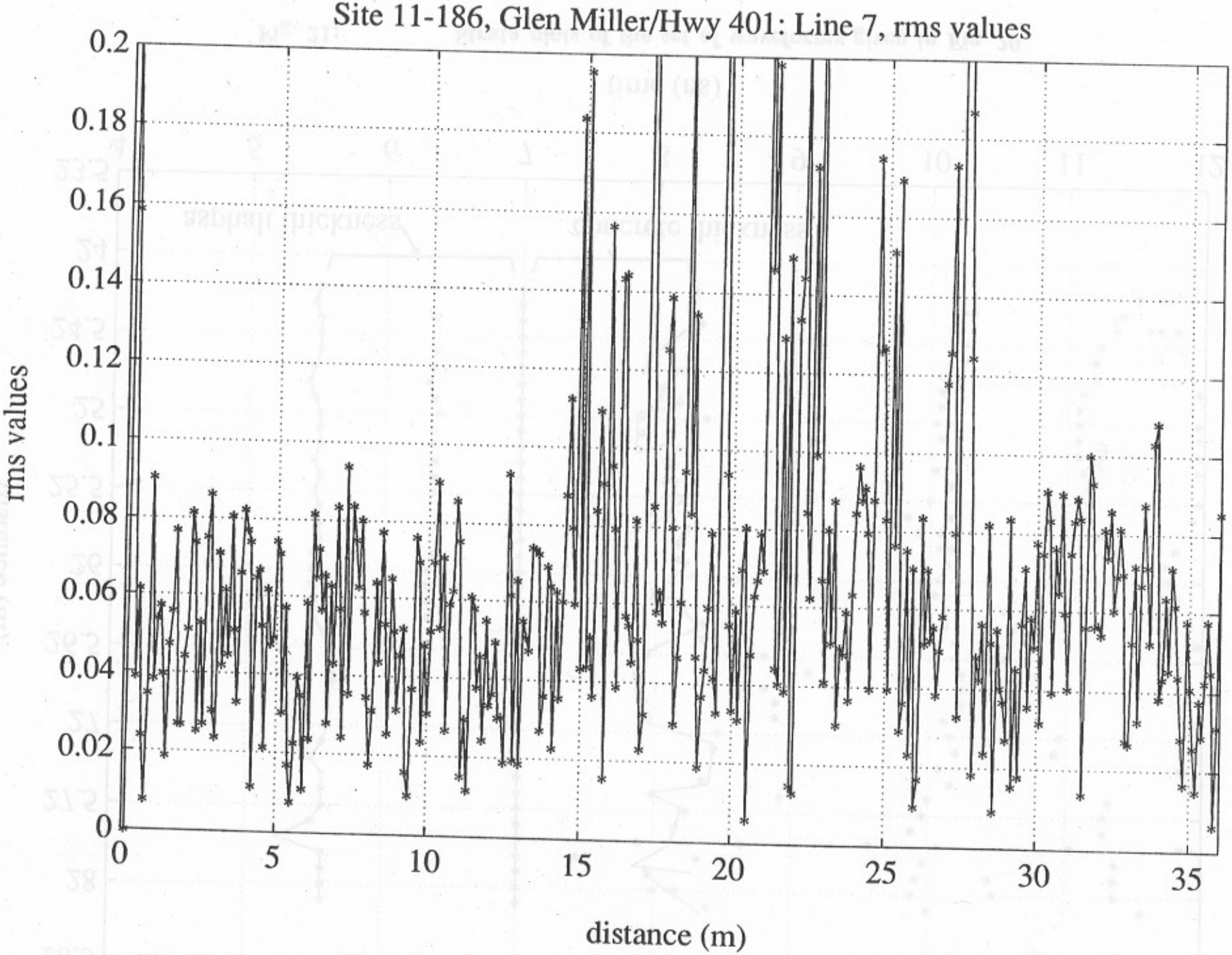

Fig. 22: **The magnitude plot of the rms values after waveform differencing along line 7.**

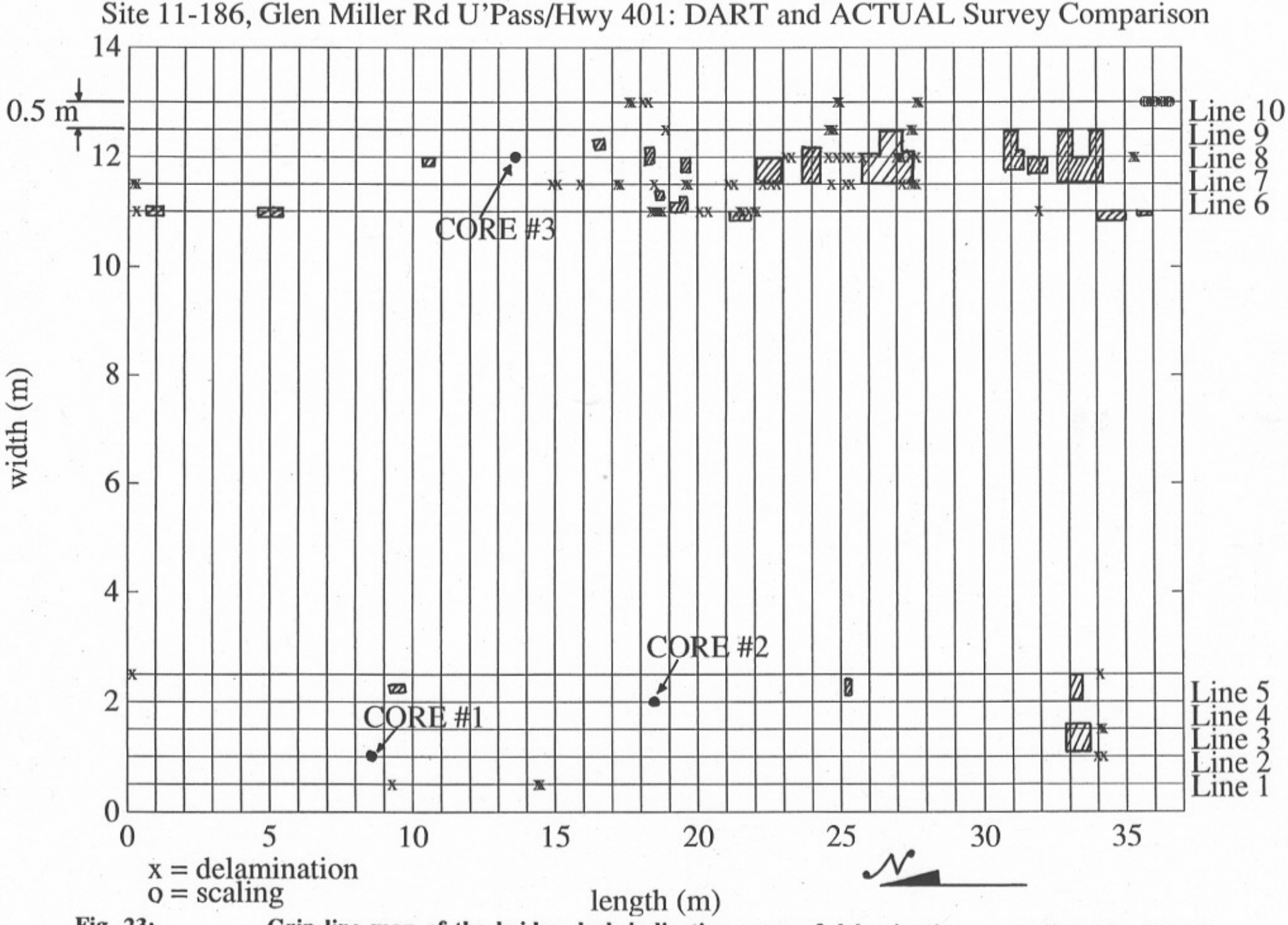

Fig. 23: **Grip line map of the bridge deck indicating areas of delamination as predicted by DART survey (symbol 'x') and actual survey (shaded area). Note the locations of the three core samples are also marked on the map.**

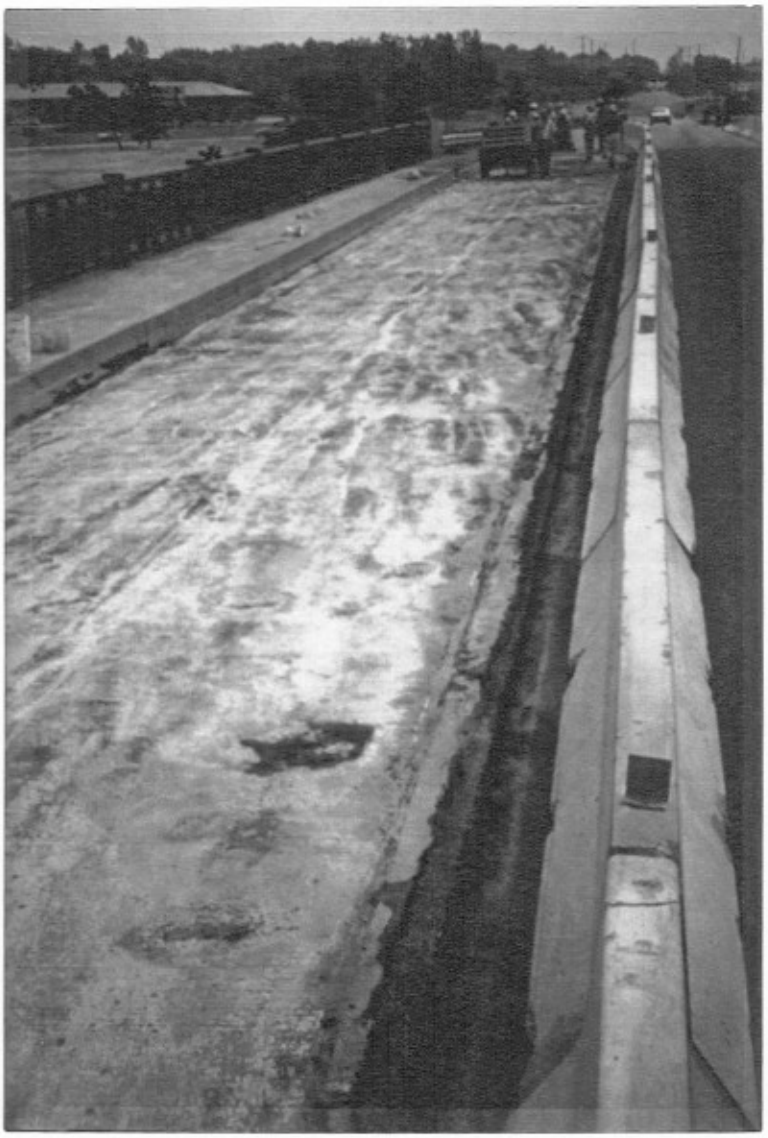

Fig. 24: **Photograph of the exposed concrete deck (with asphalt cover removed) along the Northbound lane looking south.**

(a)

(b)

Fig. 25(a)-(b): Photographs of the exposed concrete deck (looking south) along line 7.
(a) from 18 m to 22 m from the north end joint.
(b) from 22 m to 26 m from the north end joint.

(c)

(d)

Fig. 25(c)-(d): Photographs of the exposed concrete deck (looking south) along line 7.
(c) from 26 m to 28 m from the north end joint.
(d) from 33 m to 35 m from the north end joint.